Dual Regioselective Targeting the Same Receptor in Nanoparticle-Mediated Combination Immuno/Chemotherapy for Enhanced Image-Guided Cancer Treatment

Victoria O Shipunova, Elena N Komedchikova, Polina A Kotelnikova, Ivan V Zelepukin, Alexey A Schulga, Galina M Proshkina, Elena I Shramova, Hilliard L Kutscher, Georgij B Telegin, Andrei V Kabashin, et al.

▶ **To cite this version:**

Victoria O Shipunova, Elena N Komedchikova, Polina A Kotelnikova, Ivan V Zelepukin, Alexey A Schulga, et al.. Dual Regioselective Targeting the Same Receptor in Nanoparticle-Mediated Combination Immuno/Chemotherapy for Enhanced Image-Guided Cancer Treatment. ACS Nano, 2020, 14 (10), pp.12781-12795. 10.1021/acsnano.0c03421 . hal-03163227

HAL Id: hal-03163227
https://hal.science/hal-03163227

Submitted on 9 Mar 2021

HAL is a multi-disciplinary open access archive for the deposit and dissemination of scientific research documents, whether they are published or not. The documents may come from teaching and research institutions in France or abroad, or from public or private research centers.

L'archive ouverte pluridisciplinaire **HAL**, est destinée au dépôt et à la diffusion de documents scientifiques de niveau recherche, publiés ou non, émanant des établissements d'enseignement et de recherche français ou étrangers, des laboratoires publics ou privés.

Dual Regioselective Targeting the Same Receptor in Nanoparticle-Mediated Combination Immuno/Chemotherapy for Enhanced Image-Guided Cancer Treatment

Victoria O. Shipunova[†,‡], Elena N. Komedchikova[†], Polina A. Kotelnikova[†], Ivan V. Zelepukin[†,‡], Alexey A. Schulga[†], Galina M. Proshkina[†], Elena I. Shramova[†], Hilliard L. Kutscher[§,¶,‖], Georgij B. Telegin[†], Andrei V. Kabashin[#,‡*], Paras N. Prasad[‡,§*] & Sergey M. Deyev[†,‡]*

[†]Shemyakin–Ovchinnikov Institute of Bioorganic Chemistry, Russian Academy of Sciences, 16/10 Miklukho-Maklaya Street, Moscow, 117997, Russia

[‡]MEPhI (Moscow Engineering Physics Institute), Institute of Engineering Physics for Biomedicine (PhysBio), 31 Kashirskoe shosse, Moscow, 115409, Russia

[§]Institute for Lasers, Photonics and Biophotonics, University at Buffalo, 428 Natural Science Complex, Buffalo, NY, 14260-3000, USA

[¶]Department of Medicine, University at Buffalo, 875 Ellicott Street, Buffalo, NY 14203, USA

[‖]Department of Anesthesiology, University at Buffalo, 77 Goodell Street, Suite 550, Buffalo, NY 14203, USA

[#]Aix Marseille University, CNRS, LP3, Campus de Luminy – case 917, 13288, Marseille Cedex 9, France

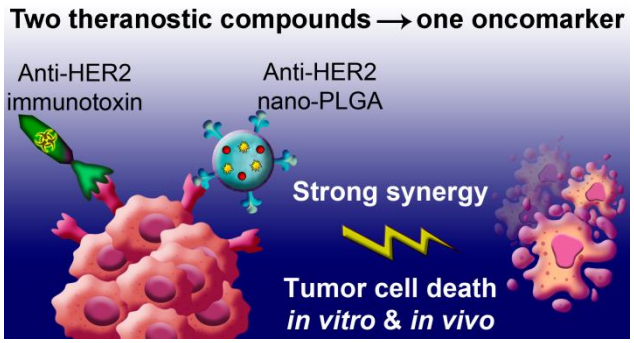

Abstract

When combined with immunotherapy, image-guided targeted delivery of chemotherapeutic agents is a promising direction for combination cancer theranostics, but this approach has so far produced only limited success due to a lack of molecular targets on the cell surface and low therapeutic index of conventional chemotherapy drugs. Here, we demonstrate a synergistic strategy of combination immuno/chemotherapy in conditions of dual regioselective targeting, implying vectoring of two distinct binding sites of a single oncomarker (here, HER2) with theranostic compounds having a different mechanism of action. We use: (i) PLGA nanoformulation, loaded with an imaging diagnostic fluorescent dye (Nile Red) and a chemotherapeutic drug (doxorubicin), and functionalized with affibody $Z_{HER2:342}$ (8 kDa); (ii) bifunctional genetically engineered DARP-LoPE (42 kDa) immunotoxin comprising of a low-immunogenic modification of therapeutic Pseudomonas exotoxin A (LoPE) and a scaffold targeting protein, DARPin9.29 (14 kDa). According to the proposed strategy, the first chemotherapeutic nanoagent is targeted by the affibody to subdomain III and IV of HER2 with 60-fold specificity compared with non-targeted particles, while the second immunotoxin is effectively targeted by DARPin molecule to subdomain I of HER2. We demonstrate that this dual targeting strategy can enhance anticancer therapy of HER2-positive cells with a very strong synergy, which made possible 1000-fold decrease of

effective drug concentration *in vitro* and a significant enhancement of HER2 cancer therapy compared to monotherapy *in vivo*. Moreover, this therapeutic combination prevented the appearance of secondary tumor nodes. Thus the suggested synergistic strategy utilizing dual targeting of the same oncomarker, could give rise to efficient methods for aggressive tumors treatment.

Keywords

HER2, PLGA, targeted delivery, theranostics, affibody, DARPin, immunotoxin

Being one of the major threats for humankind, cancer requires diagnosis and intervention at the very early stages of its development, and timely treatment. The situation is especially critical in cases of aggressive tumors, which rapidly grow and provoke the appearance of metastasis. In these cases, non-specific chemotherapy drugs such as doxorubicin, paclitaxel, methotrexate, *etc*. are typically applied at high dosages to initiate extensive cancer cell kill, but such therapy can lead to severe side effects such as myelosuppression, chronic cardiotoxicity, hepatotoxicity, neurotoxicity and many others.[1–3] To enhance antitumor treatment efficiency and reduce side effects, different monotherapies can be combined – such as chemotherapy, radiotherapy, cell therapy, or immunotherapy.[4] For example, chemotherapy could be applied in combination with immunotherapy based on the use of highly toxic immunotoxins, which are typically vectored into the tumor and metastasis to initiate additional cancer cell kill.[5–8] The combination therapy efficiency can be further enhanced by the employment of nanoparticles as drug carriers,[9–11] which makes possible the increase of local drug concentration and enable additional imaging and therapy functionalities based on unique physicochemical properties of nanomaterials.[12–14] In this case,

active nanoparticle targeting strategies are usually applied *via* decoration of particle surface by specific ligands for cognate receptors expressed on the intended target cell type.[10,15]

Significant efforts have been applied in recent years on the design of targeting molecules, which could specifically bind to cancer-associated receptors, and thus selectively deliver theranostic agents to cancer cells to initiate their elimination.[16,17] Full-size IgG antibodies are so far the most popular targeting molecules used for both imaging[18] and therapy[19] tasks, but these molecules are relatively large (150 kDa, 7-14 nm) and can significantly affect the immune response of the organism. The targeting effectiveness can be further enhanced by using newly-emerging targeting scaffold proteins such as DARPins[20,21] and affibodies,[22,23] which are much smaller (14-18 kDa and 6–8 kDa, *ca.* 5–7 nm and 3–4 nm, respectively) and can offer a series of advantages, including high affinity, low immunogenicity, excellent solubility, and thermodynamic stability.

Several recent studies reported the development of dual targeting strategies when one or two targeting modalities are used to deliver drugs to tumors to perform combination therapies (*e.g.*, chemo/immunotherapy). In this case, specially designed molecules and supramolecular structures are used to target different overexpressed oncomarkers. Some reports describe the design of nanoagents modified with two ligands for different receptors, *e.g.*, folate and transferrin modified liposomes loaded with doxorubicin,[24] or the use of full-size bispecific antibodies directed toward different cell surface receptors and/or soluble factors such as HER2 & EpCAM or EGFR & IL-13R.[25] Other studies describe targeting of one receptor with two molecular compounds, *e.g.*, with anti-EGFR antibody cetuximab and tyrosine kinase inhibitor of tumors overexpressing EGFR in native and mutant forms.[26] The application of dual targeting strategies makes possible the improvement of treatment efficiency and specificity, as well the minimization of side effects, but these technologies had so far a limited success due to the biological complexity of cancer

molecular networks and a variety of its manifestations. To further advance these technologies, one has to address a series of issues, including the possible appearance of secondary tumor nodes after the elimination of primary tumor, rapidly developing drug resistance of metastatic tumors due to mutations and genetic polymorphism, and systemic toxicity and immunogenicity for re-treated patients. To further complicate the situation, cancer cells are often characterized by the overexpression of a single cell-receptor target, and thus there is no way to improve cell specificity by targeting multiple receptors on the same cell. This situation often takes place in the case of the HER2 oncomarker, a member of the EGFR receptor family,[27–29] whose overexpression often correlates with patients' resistance to chemotherapy, high recurrence of disease, high tumor metastatic potential and poor prognosis.[30] This happens in 20-30% of human breast cancer cases, as well as in the cases of bladder carcinomas, gallbladder, extrahepatic cholangiocarcinomas, cervical carcinomas, and other malignancies predominantly of epithelial origin.[27] To meet all these challenges, a technology combining intelligent targeting with prompt aggressive elimination of tumors *via* different mechanisms of cancer cell kill is still needed.

Here, we demonstrate a synergistic strategy of dual regioselective targeting, implying vectoring of two distinct binding sites of a single HER2 oncomarker, with theranostic compounds having different mechanisms of action (chemo- and immunotherapeutic agents, one of which enables image-guiding). By applying such a strategy, we demonstrate: 1) high specificity of theranostic agents towards HER2-overexpressing cancer cells with up to 100% cell death; and 2) 1000-fold reduction of the effective concentration of our highly potent immunotoxin. Moreover, we show that this dual targeting strategy significantly improves the efficacy of anticancer therapy of HER2-positive cells *in vivo* compared to monotherapy, and prevents the appearance of secondary tumor

nodes. We believe that this synergistic strategy can provide a significant improvement of therapeutic efficiency, thus giving rise to alternative pathways to treat aggressive tumors.

Results and Discussion

Experimental design

Our architecture for the implementation of combined immune/chemotherapy is schematically represented in **Fig. 1**.

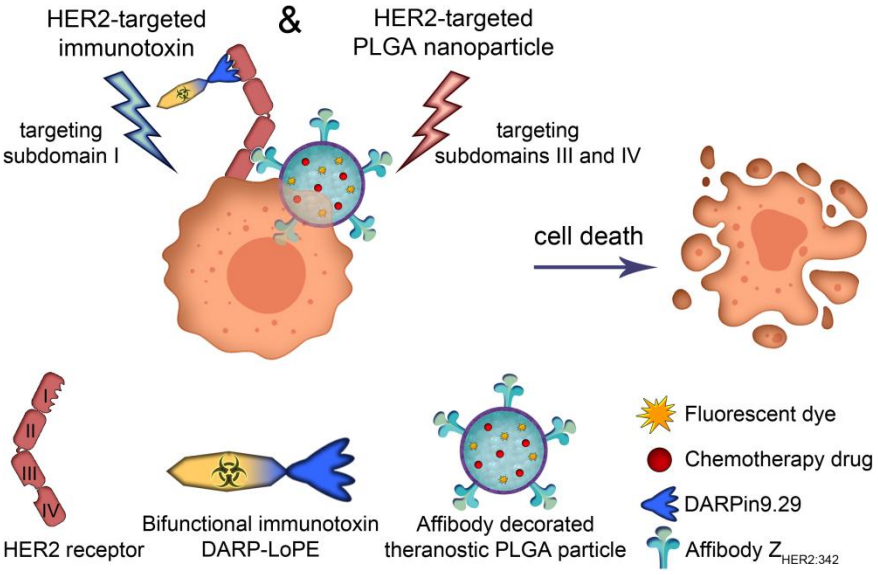

Figure 1. *Combination cell therapy with targeted nanoparticle PLGA*$Z_{HER2:342}$ and targeted immunotoxin DARP-LoPE. PLGA nanoparticles are loaded with Nile Red (diagnostic) and doxorubicin (therapeutic) and modified with HER2-recognizing scaffold protein, affibody $Z_{HER2:342}$. Immunotoxin consists of DARPin9.29 – HER2-specific scaffold protein and low-immunogenic modification of Pseudomonas exotoxin A (LoPE), which induces cell apoptosis.*

This architecture includes two relevant agents:

1) *Targeted chemotherapy agent*. This agent is based on poly(lactic-co-glycolic acid) (PLGA) nanoparticles as a primary building block. PLGA is composed of lactic and glycolic acids, which

are presented in the organism and are biocompatible and biodegradable. To enable cytotoxic chemotherapy, PLGA nanoparticles are loaded with doxorubicin (Dox), a potent anthracycline antibiotic that intercalates between two base pairs of the DNA and inhibits topoisomerase II, thus providing the cytostatic effect. To enable diagnostic capability, the nanoparticles are incorporated with a water-insoluble dye, 9-diethylamino-5-benzo[α]phenoxazinone (Nile Red), with excitation and emission wavelengths suitable for most *in vitro* and *in vivo* imaging devices. To achieve targeted chemotherapy, PLGA nanoparticle-based complex is conjugated with an affibody $Z_{HER2:342}$, a synthetic polypeptide of non-immunoglobulin origin. Affibody molecules represent an original class of recognizing proteins that are selected by the phage display method from the 58-amino acid three helical domain derived from the immunoglobulin-binding staphylococcal protein A.[31] Such non-immunoglobulin scaffold-based affinity proteins are characterized by their exceptional stability in biological fluids and low immunogenicity.[23] Affibody $Z_{HER2:342}$ with an affinity of 22 pM binds the HER2 receptor, namely to the junction of domains III and IV of the receptor,[32,33] and was shown to be an excellent candidate for HER2 breast tumor imaging and treatment, both in experimental animals and cancer patients.[32,34,35]

Moreover, its N- and C-terminus are available for chemical conjugation and genetic modifications. In our study, PLGA nanoparticles were synthesized by a water-oil-water double emulsion method. Functional theranostic and targeting agents were added *via* further hierarchically assemblying of PLGA nanoparticle. Details of synthesis and functionalization of PLGA-based nanocomplexes are described in the Materials and Methods section.

2) *Targeted immunotherapy agent*. This agent consists of a scaffold protein DARPin9.29, which binds to the domain I of the HER2 receptor, and a low-immunogenic modification of Pseudomonas exotoxin A (LoPE), which blocks eukaryotic elongation factor II (**Fig. 1**), to get the immunotoxin

DARP-LoPE.[36,37] DARP-LoPE is highly potent with an IC50 = 15 pM for HER2-positive cells.[36] Since DARPin9.29 binds to another domain of the HER2 receptor,[38] specifically, domain I, it can be used in combination with targeted PLGA particles without any steric hindrance.

In our study, we applied the combination of described targeting supramolecular agents for image-guided treatment of HER2-overexpressing cancer cells both *in vitro* and *in vivo* (**Fig. 1**).

Characterization of PLGA nanoparticle-based complexes

As follows from scanning electron microscopy data, as-synthesized PLGA nanoparticles present monodisperse structures having a shape close to spherical with a mean diameter and standard deviation of 140 ± 30 nm, according to SEM image processing (**Fig. 2a** and **Fig. S1**).

Fig. 2b presents excitation and emission spectra of PLGA nanoparticles in phosphate-buffered saline (PBS). One can see that fluorescence from the samples corresponded to that of the loaded Nile Red dye. Dynamic and electrophoretic light scattering methods showed that the hydrodynamic size of PLGA nanoparticles was 182 ± 54 nm in PBS (**Fig. 2c**), while the ζ-potential was equal to –1.08 ± 0.10 mV in 10 mM KNO_3 (**Fig. 2d**). Doxorubicin loading efficiency was found to be 4.8 nM of Dox per 1 g of PLGA nanoparticles. The doxorubicin release profile exhibits any initial burst in drug release during the first 20 mins, then the drug release stopped and remained at a constant ratio (**Fig. S2**). The Dox release was found not to exceed 30 % of the total drug content in a wide pH range (2-7) for 30 h at room temperature. Such sustained release was achieved *via* chitosan stabilization of the nanoparticle surface and is in good agreement with other previously published studies.[39]

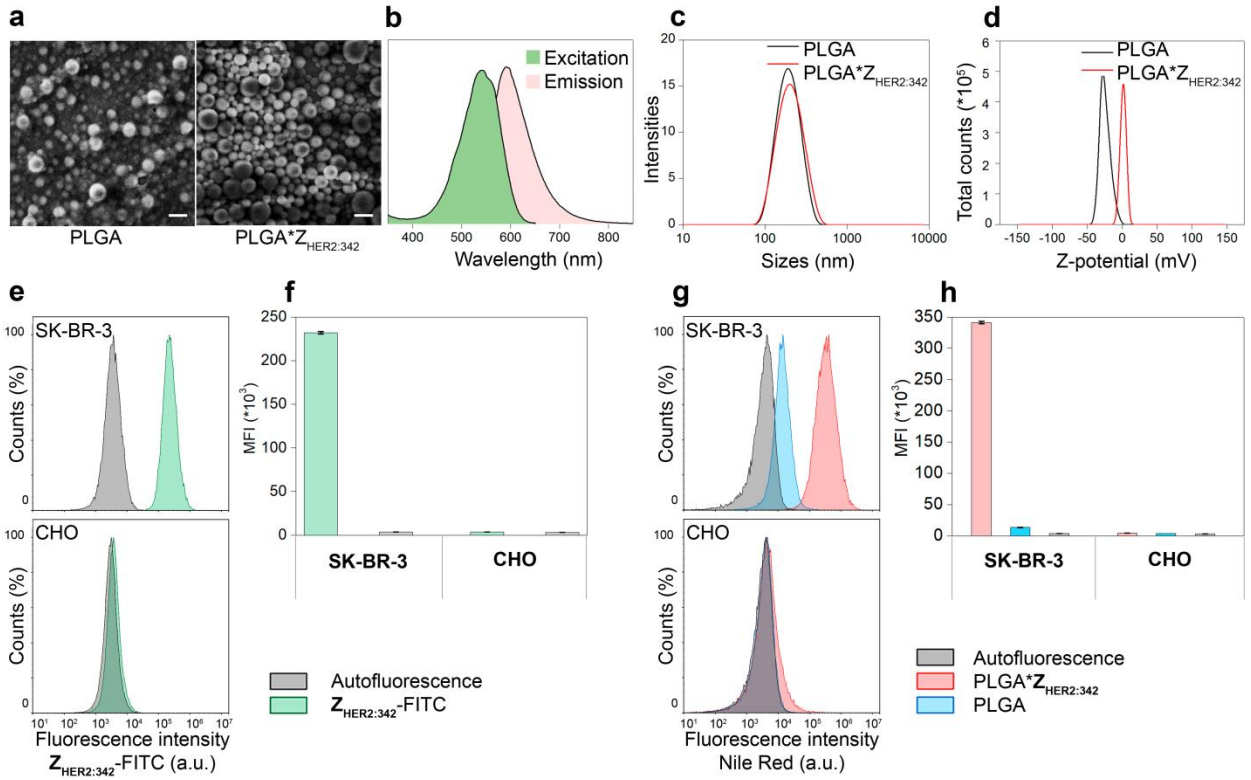

Figure 2. *Characterization and conjugation of PLGA nanoparticles to $Z_{HER2:342}$, and cell-binding assays.* ***a,*** *Scanning electron microscopy images of PLGA nanoparticles before and after conjugation with $Z_{HER2:342}$. Scale bar, 500 nm.* ***b,*** *Normalized excitation (emission 670 nm) and emission (excitation 490 nm) spectra of the PLGA nanoparticles.* ***c,*** *Hydrodynamic size distribution of PLGA and PLGA*$Z_{HER2:342}$ nanoparticles obtained from DLS measurements.* ***d****, ζ-potential distribution of PLGA and PLGA*$Z_{HER2:342}$ nanoparticles obtained from electrophoretic light scattering measurements.* ***e,*** *Flow cytometry assay to evaluate $Z_{HER2:342}$-FITC bound to cells. Flow cytometry histograms were obtained in BL1 channel (excitation laser 488 nm, emission filter 530/30 nm). Autofluorescence is shown by grey, cells labeled with $Z_{HER2:342}$-FITC are shown by red.* ***f****, Median fluorescence intensities of cells labeled with $Z_{HER2:342}$-FITC.* ***g****, Flow cytometry assay: evaluation of PLGA and PLGA*$Z_{HER2:342}$ nanoparticles bound to cells. Flow cytometry histograms were acquired in YL2 channel (excitation laser 561 nm, emission filter 615/20 nm). Autofluorescence is shown by grey, cells labeled with PLGA*$Z_{HER2:342}$ nanoparticles are shown by red, cells labeled with pristine PLGA nanoparticles are shown by blue.* ***h****, Median fluorescence intensities of cells labeled with PLGA and PLGA*$Z_{HER2:342}$.*

To make PLGA nanoparticles capable of targeting HER2 receptors, they were conjugated with affibody $Z_{HER2:342}$ molecules according to a procedure described in the Materials and Methods section. As shown in **Fig. 2c,** the mean hydrodynamic diameter of nanoparticles increased from

182 ± 54 nm to 186 ± 65 nm after their conjugation with $Z_{HER2:342}$, suggesting the immobilization of small protein affibody on the particle surface. As shown in **Fig. 2d,** ζ-potential of conjugated nanoparticles demonstrated a significant change from –1.08 ± 0.10 mV to –23.4 ± 1.4 mV (**Fig. 2d**), evidencing a high conjugation efficiency. Thus, PLGA nanoparticles after conjugation with affibody retain their colloidal stability and shape, which was confirmed not only by visual observation and DLS measurements, but also with scanning electron microscopy (**Fig. 2a**). The protein content on the surface of PLGA conjugates measured by BCA protein assay was found to be 7.2 μg per 1 mg of PLGA (see the detailed description of measurement procedure in the Materials and Methods section).

HER2–overexpressing cells labeling and imaging with PLGA*$Z_{HER2:342}$ nanoparticles

To evaluate the efficacy of obtained PLGA*$Z_{HER2:342}$ nanoparticles in imaging and killing of HER2–overexpressing cancer cells, we selected two different cell lines for *in vitro* experiments: SK-BR-3 and CHO. SK-BR-3 cells are breast adenocarcinoma that overexpresses HER2 (about 10^6 receptors per cell[40]), while CHO cells are Chinese hamster ovary cells that do not express any EGFR receptors. HER2 expression on the selected cells was confirmed with flow cytometry measurements by their labeling with fluorescent anti-HER2 full-size antibody Trastuzumab-FITC (see **Fig. S3,S4** and **Note S1**).

First, we evidenced the specificity of interaction between the purified affibody $Z_{HER2:342}$ and HER2 receptors on the cell surface. We conjugated $Z_{HER2:342}$ with a fluorescent dye FITC, to get $Z_{HER2:342}$-FITC. Cells were incubated with $Z_{HER2:342}$-FITC and assessed by flow cytometry (**Fig. 2e,f**). Flow cytometry histograms shown in **Fig. 2e** demonstrate that $Z_{HER2:342}$-FITC interacts only with HER2–

overexpressing SK-BR-3 cells. As follows from the analysis of median fluorescence intensities (MFI) of labeled cell populations shown in **Fig. 2f**, the ratio of $Z_{HER2:342}$-FITC bound to SK-BR-3 cells *versus* CHO cells was equal to 61.5, suggesting a high specificity of $Z_{HER2:342}$ to SK-BR-3 cells.

Next, we exposed SK-BR-3 and CHO cells to PLGA*$Z_{HER2:342}$ or PLGA nanoparticles and evaluated the cell labeling efficiency *via* flow cytometry (**Fig. 2g,h**). Our tests showed that MFI of SK-BR-3 cells incubated with PLGA*$Z_{HER2:342}$ was 81.4 fold higher than the relevant parameter in the case of CHO cells. In contrast, there was no difference in the uptake of PLGA nanoparticles (**Fig. 2h)**. These data confirm a high specificity of PLGA*$Z_{HER2:342}$ nanoparticles to HER2–overexpressing SK-BR-3 cells.

To assess the imaging potential, we incubated cells with Nile Red-loaded PLGA*$Z_{HER2:342}$ nanoparticles and Hoechst 33342 dye (dsDNA dye), which is efficient in staining the nuclei of living cells. As shown in **Fig. 3a**, PLGA*$Z_{HER2:342}$ nanoparticles are indeed efficient in imaging HER2–overexpressing cells *in vitro.* The intracellular fate of PLGA*$Z_{HER2:342}$ was studied using confocal scanning microscopy. Cell endosomes were labeled by cell transfection with CellLight Early Endosomes-GFP, BacMam 2.0; cell lysosomes were labeled with LysoTracker DeepRed. It was found (**Fig. 3b**) that PLGA*$Z_{HER2:342}$ nanoparticles start to internalize inside cells 15 min after incubation and colocalize with early endosomes. 4h later, PLGA*$Z_{HER2:342}$ are localized in lysosomes, thus realizing HER2-receptor mediated endocytosis with final transfer to lysosomes.

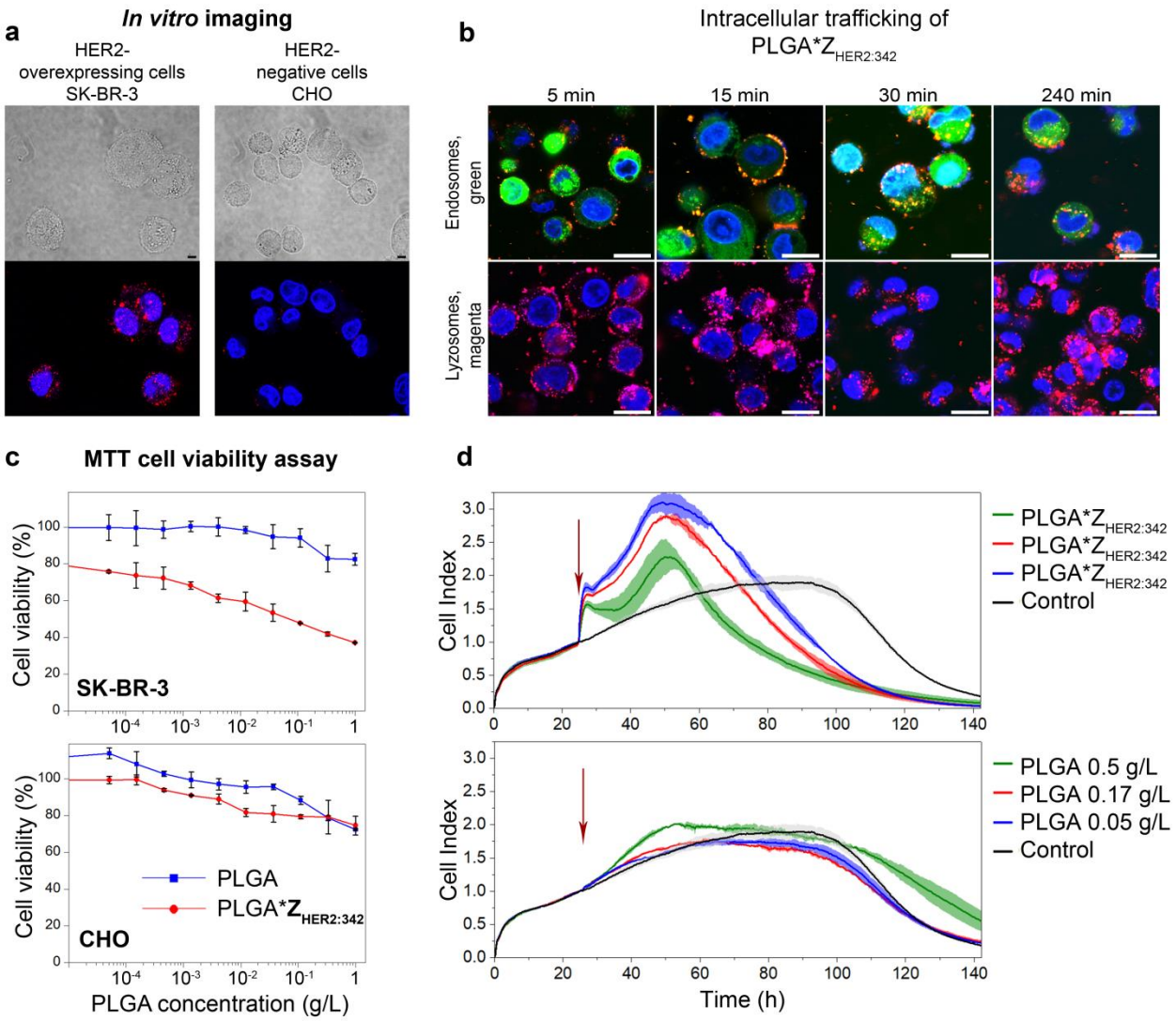

Figure 3. *Cellular imaging and cytotoxicity of the chemotherapy agent.* ***a,*** *Confocal laser scanning microscopy images confirming uptake of PLGA*Z$_{HER2:342}$ nanoparticles by SK-BR-3 cells, but not by CHO cells. Top panels show bright-field images of SK-BR-3 and CHO cells, and bottom panels show overlaid confocal images of cells labeled with PLGA*Z$_{HER2:342}$ nanoparticles and Hoechst 33342 (Hoechst 33342: excitation laser 405 nm, emission filter 440/40 nm; PLGA: excitation laser 561 nm, emission filter 600/52 nm). Scale bars, 5 μm.* ***b,*** *Intracellular trafficking of PLGA*Z$_{HER2:342}$ nanoparticles. Endosomes are labeled with GFP: excitation laser 488 nm, emission filter 440/40 nm; PLGA: excitation laser 561 nm, emission filter 600/52 nm; lysosomes: excitation laser 642 nm, emission filter 647LP nm; Hoechst 33342: excitation laser 405 nm, emission filter 440/40 nm).* ***c****, MTT assay results on the interaction of PLGA and PLGA*Z$_{HER2:342}$ nanoparticles with SK-BR-3 and CHO cell lines. Cell viability is presented in % in comparison with non-treated control cells.* ***d,*** *Real-time cell analysis. Influence of three concentration of targeted PLGA*Z$_{HER2:342}$ and non-targeted PLGA particles on growth kinetics of SK-BR-3 cells during 140 hours. Arrows indicate the time when nanoparticles were injected into E16 xCELLigence plates.*

Cytotoxicity of PLGA$Z_{HER2:342}$ nanoparticles*

To determine whether targeted PLGA*$Z_{HER2:342}$ nanoparticles have a specific cytotoxic effect, we incubated SK-BR-3 and CHO cells with different concentrations of PLGA and PLGA*$Z_{HER2:342}$ nanoparticles and assessed cytotoxicity after 48 h by MTT. As shown in **Fig. 3c**, PLGA*$Z_{HER2:342}$ nanoparticles exhibited specific cytotoxic effect only for HER2–overexpressing SK-BR-3 cells. The IC50 value for PLGA*$Z_{HER2:342}$ nanoparticles in SK-BR-3 cells was 80 μg/mL. To assess the effect of targeted nanoparticles on the rate of HER2-positive cell growth, we performed a real-time cell analysis using the xCelligence RTCA system (Acea). Cells were seeded onto slides and allowed to attach and grow for 24 h. Then, different concentrations of PLGA or PLGA*$Z_{HER2:342}$ nanoparticles were added to wells. As follows from our tests, the presence of PLGA*$Z_{HER2:342}$ nanoparticles affect only the growth of SK-BR-3 cells. Here, we observed a significant increase in cell index during the first 20 h after nanoparticle addition, which could be explained by nanoparticle binding to the cells, resulting in an increased impedance of the surface layer (**Fig. 3d**). In comparison, non-targeted PLGA nanoparticles provided similar cell growth kinetics as non-treated control cells. During the following 100 h, cell index decreased due to cell death.

In vitro assessment of combination cancer cell therapy using PLGA$Z_{HER2:342}$ nanoparticles and immunotoxin*

To enhance the targeted cytotoxic effect of doxorubicin-loaded PLGA*$Z_{HER2:342}$ nanoparticles, we combined this agent with our original immunotoxin DARP-LoPE. First, we evaluated the specificity of DARP-LoPE binding to HER2-positive cells. DARP-LoPE was modified with FITC,

incubated with SK-BR-3 and CHO cells, visualized with confocal microscopy (**Fig. 4a**), and finally quantified using flow cytometry (**Fig. 4b**). As shown in **Fig. 4,** DARP-LoPE bound only to HER2-overexpressing SK-BR-3 cells.

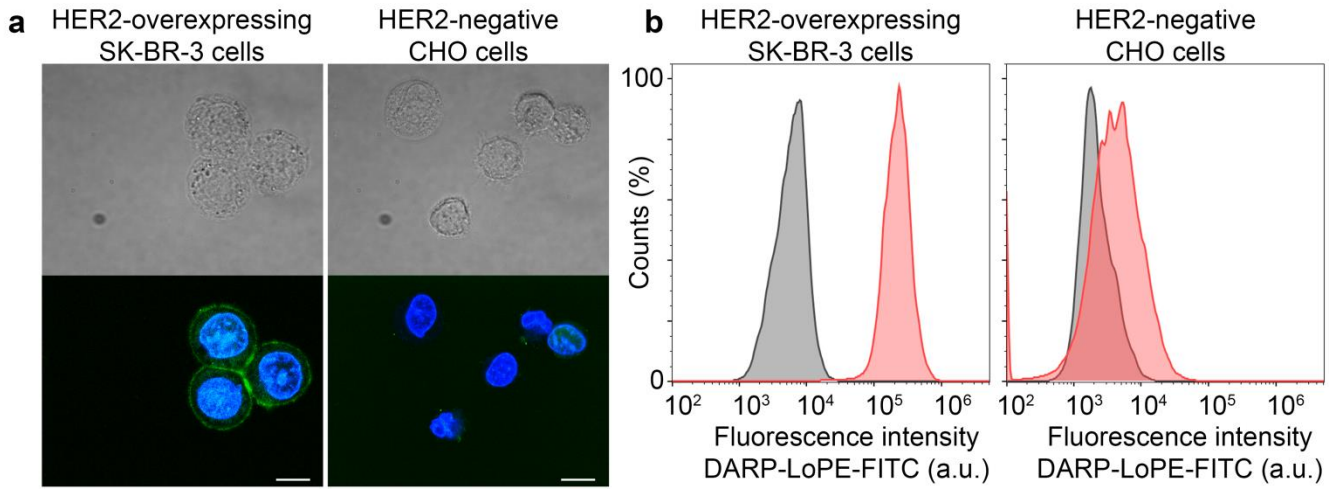

Figure 4*. In vitro assessment of DARP-LoPE immunotherapy agent.* ***a,*** *Confocal laser scanning microscopy images confirming the specific labeling of SK-BR-3 cells with DARP-LoPE-FITC. Top panels show bright-field images of SK-BR-3 and CHO cells, and bottom panels present overlaid confocal images of cells incubated with DARP-LoPE-FITC and Hoechst 33342 (Hoechst 33342: excitation laser 405 nm, emission filter 440/40 nm; DARP-LoPE-FITC: excitation laser 488 nm, emission filter 525/45 nm). Scale bars, 20 µm.* ***b****, Flow cytometry assay to evaluate DARP-LoPE-FITC bound to cells. Flow cytometry histograms acquired in FL1 channel (excitation laser 488 nm, emission filter 525/20 nm): autofluorescence is shown by grey, cells labeled with DARP-LoPE-FITC are shown by red.*

Efficient cancer treatment strategies imply minimization of negative effects on healthy cells. As we showed earlier,[36,37] targeted immunotoxin DARP-LoPE has a pronounced cytotoxic effect on HER2–overexpressing cells, but its effect on cells with a normal HER2 receptor expression has yet to be clarified. HER2 is presented in many types of healthy human cells at 2-3 order of magnitude lower quantities (https://www.proteinatlas.org/). We investigated the cytotoxic effect of DARP-LoPE in combination with PLGA*$Z_{HER2:342}$ and non-targeted PLGA nanoparticles. For

this purpose, we added to the experimental setup A549 lung epithelial carcinoma cells, which possess a normal level of HER2 expression. HER2 expression on A549 cells was assessed using flow cytometry by their labeling with anti-HER2 full-size antibody, Trastuzumab-FITC (see **Fig. S4)**. The MFI of A549 cells labeled with $Z_{HER2:342}$-FITC was 12188. For comparison, the MFI of SK-BR-3 and CHO cells was 231896 and 3771, respectively. Additionally, in our experimental setup, all selected cell lines exhibited similar sensitivity to doxorubicin (**Fig. S5**). This fact is essential for a correct comparison and interpretation of cytotoxic effects from selected agents.

To evaluate the correlation between the level of HER2 cell expression and efficiency of targeted cell kill by PLGA*$Z_{HER2:342}$ nanoparticles, we investigated the DNA content in cell cycle phases using a flow cytometry method. The DNA content in the *sub*-G1 phase (containing cells with fragmented DNA, *e.g.*, apoptotic cells) was in good correlation with cellular uptake of PLGA*$Z_{HER2:342}$ with HER2 expressing cell lines, with the efficiency depending on the expression level. For A549 cells with normal HER2 expression, the percentage of cells in *sub*-G1 phase was, *e.g.*, for the medium tested PLGA*$Z_{HER2:342}$ concentration (0.1 g/L), 22 times smaller than this value for SK-BR-3 cells, namely 52.6% for SK-BR-3 *versus* 2.4% for A549. Comparing these values with a sub-G1 percentage of untreated A549 cells (2.01%), one can see that it is possible to use the concentration of targeted PLGA nanoparticles that is non-toxic for normal cells and quite effective for HER2-overexpressing cells killing. Moreover, we did not detect any significant effect on DNA content in the *sub*-G1 for HER2–negative CHO cells (**Fig. S6**).

We then used an MTT assay to evaluate the combined action of PLGA*$Z_{HER2:342}$ and DARP-LoPE on the viability of cells exhibiting different HER2 expression levels. DARP-LoPE was mixed with PLGA and PLGA*$Z_{HER2:342}$ nanoparticles at fixed concentration of 80 μg/mL (equal to IC50 of nanoparticles) and then incubated with SK-BR-3, A549, and CHO cell cultures (**Fig. 5a-c**).

The MTT assay was performed after 48 h of incubation. To compare the efficacy of combination therapy with that of the targeted immunotoxin alone, we evaluated the concentration of immunotoxin that was needed to achieve 65% cell death (or 35% cell survival). We used this criterion because in both cases (*i.e.*, DARP-LoPE or DARP-LoPE & PLGA*$Z_{HER2:342}$), the dose-effect curve was non-sigmoidal, making it difficult to estimate 50% cell death. Moreover, 35% cell survival rate was in the linear region of the cytotoxicity curve in both cases. Using this criterion, we found that to achieve 65% cell death (35% of survived cells), DARP-LoPE immunotoxin concentration of 1.7 nM was needed. On the other hand, when combined with targeted the PLGA*$Z_{HER2:342}$ nanoparticles, this concentration was lowered by 944-fold, down to 1.8 pM.

A significant change in cytotoxicity of the combination of targeted drugs stimulated us to study possible any synergetic effect of these agents. To perform this study, the Chou-Talalay method[41,42] and the CompuSyn software program (ComboSyn Inc., Paramus, NJ. U.S.A.) were used, which are efficient in calculating the combination index (CI) and dose reduction index (DRI) for two or more independent drugs at different concentrations of these drugs. Here, CI = 1 indicates an additive effect, CI < 1 indicates synergism, CI > 1 indicates antagonism; and DRI = 1 indicates no dose reduction, DRI < 1 indicates favorable drug dose reduction, and DRI > 1 indicates not favorable dose reduction. Since this method is applicable only for independent drugs, first of all, we performed *in situ* tests which show that PLGA*$Z_{HER2:342}$ and DARP-LoPE do not interact with each other in a wide concentration range (Fig. S7), which makes the use of this method legitimate.

Next, CI values for the combination of PLGA*$Z_{HER2:342}$ and DARP-LoPE were calculated for fixed PLGA*$Z_{HER2:342}$ concentration and varied DARP-LoPE concentrations for three cell lines: SK-BR-3, A549, and CHO cells (Note S2). CI values revealed very strong synergism/strong synergism

(CI ranging from 0.003 to 0.014) for SK-BR-3 cells, moderate synergism or nearly additive effect for A549 cells (CI from 0.097 to 0.788) and from moderate synergism to antagonism for CHO cells (CI ranged from 0.503 to 2.915). The description of CI index values (very strong synergism → strong synergism → … → additive affect → … → antagonism → very strong antagonism) was performed according to Table 4 in the description of the theoretical basis of synergism quantification method.[41]

DRI for DARP-LoPE appears to be ranged from 7.2 to 1904.1 and from 30648.4 to 15.5 for PLGA*$Z_{HER2:342}$ for SK-BR-3 cells, with much less pronounced effect on A549 cells, and unfavorable dose reduction for CHO cells (Note S2).

Despite the high efficiency of the proposed combination therapy, the MTT assay results did not report 100% cell death even at high concentrations of DARP-LoPE, for which cell viability comes to a plateau at 14% (**Fig. 5a**). No significant changes were observed even when the incubation time was increased from 48 h to 72 h (**Fig. 5d**), and cell viability reached a plateau at 9%.

To understand whether this fact is related to the survival of ~10% of the cells or to a particular manifestation of the MTT assay, we performed an additional survival test, namely, a clonogenic assay (or colony formation assay), which is much closer to *in vivo* cytotoxicity assessment than the MTT assay. In many cases, MTT reduction reflects the level of cell metabolism (namely, mitochondrial activity) rather than cell proliferation.[43] The colony formation assay could provide more sensitive and reliable results that depend predominantly on cell growth mechanisms rather than any cell membrane damage.[44,45] The clonogenic assay was performed as follows. We incubated 100 000 cells with targeted compounds for a short time (30 min), then 100-fold diluted the cells in a growth medium and cultured for 3 weeks, followed by counting grown cell colonies.

The results (number of cell colonies) were then presented depending on the initial concentration of targeted compounds before the dilution.

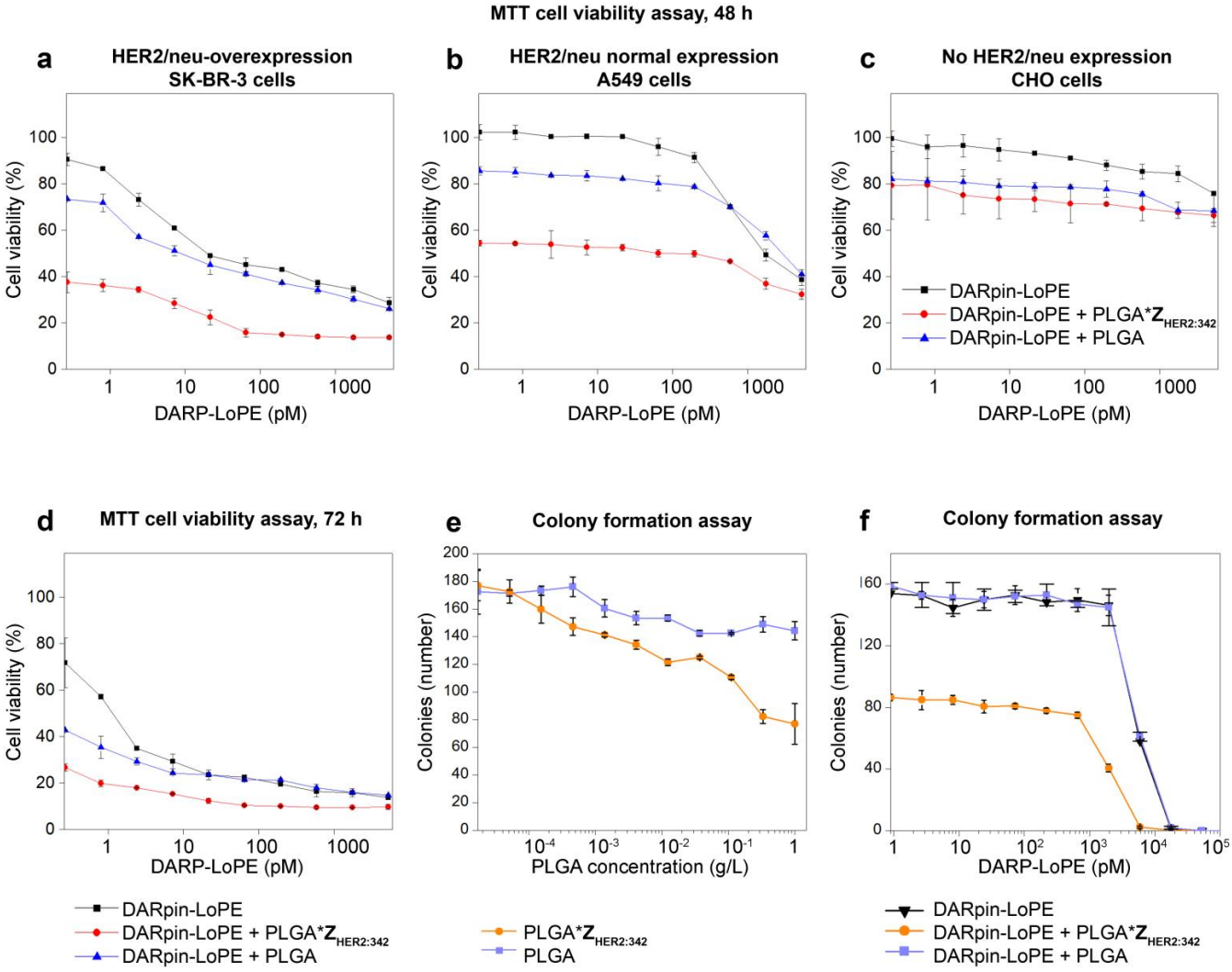

Figure 5. *Combination targeted chemo/immunotherapy in vitro. MTT assay results for DARP-LoPE, DARP-LoPE & PLGA, and DARP-LoPE & PLGA*$Z_{HER2:342}$ nanoparticles incubated with SK-BR-3* ***a****, A549* ***b,*** *and CHO* ***c,*** *cell lines, 48 h after the incubation. Cell viability is presented in % in comparison with control non-treated cells.* ***d,*** *MTT assay results for DARP-LoPE, DARP-LoPE & PLGA, and DARP-LoPE & PLGA*$Z_{HER2:342}$ nanoparticles incubated with SK-BR-3 cells, 72 h after the incubation.* ***e,*** *Colony formation assay results for PLGA and PLGA*$Z_{HER2:342}$ nanoparticles incubated with SK-BR-3 cell line.* ***f,*** *Colony formation assay results for DARP-LoPE, and DARP-LoPE & PLGA*$Z_{HER2:342}$ nanoparticles incubated with SK-BR-3 cell line.*

The cytotoxic effect was studied for SK-BR-3 cells. Colony formation assay tests showed that in the absence of immunotoxin, PLGA and PLGA*$Z_{HER2:342}$ nanoparticles provide similar results (compare **Fig. 3c** and **Fig. 5e, Fig. S8**). However, the addition of targeted immunotoxin DARP-LoPE led to a drastic improvement of cytotoxicity. As shown in **Fig. 5f, Fig. S9**, the combined action of PLGA*$Z_{HER2:342}$ and DARP-LoPE led to 100% cell death.

We also found that to achieve 65% cell death (35% of survived cells), a DARP-LoPE immunotoxin concentration of 6.76 nM was needed, while the combination of DARP-LoPE with targeted PLGA*$Z_{HER2:342}$ nanoparticles led to the decrease of effective concentration down to 1.46 nM. Thus, the results of clonogenic assay processing show that the effective concentration of DARP-LoPE could be 4.5-fold reduced under the application of targeted combination therapy.

In vivo imaging and combination cancer cell therapy with targeted nanoparticles and immunotoxin

First, we evaluated the efficiency of PLGA*$Z_{HER2:342}$ nanoparticles as markers for tumor imaging *in vivo*. For this purpose, HER2–overexpressing tumor-bearing athymic BALB/c Nude mice were administered *i.v.* with PLGA or PLGA*$Z_{HER2:342}$ nanoparticles, and then assessed by a living-animal imaging technique (using IVIS Spectrum CT, Perkin Elmer). As shown in **Fig. 6a**, PLGA*$Z_{HER2:342}$ nanoparticles were indeed efficient for *in vivo* imaging of specific HER2–overexpressing cells. Living animal images were supported by data showing average radiance per tumor area in *photons per second per* cm^2 *per steradian* (red circled area in **Fig. 6a**). As follows from these data, the ratio of targeted nanoparticles PLGA*$Z_{HER2:342}$ *versus* non-targeted ones

PLGA in the tumor was equal to 59.9 ($7.846 \cdot 10^6$ *vs.* $1.310 \cdot 10^5$ p/s/cm^2/sr), which is comparable to results of our *in vitro* tests.

Finally, the efficiency of proposed combination therapy using PLGA*$Z_{HER2:342}$ and DARP-LoPE was assessed in the treatment of HER2-positive xenograft tumor-bearing mice. Mice were injected subcutaneously with HER2-overexpressing cells (expressing NanoLuc luciferase), and after tumor reached 60-80 mm^3, they were randomly divided into 4 groups and treated with five consecutive injections every two days: 1) 100 μL of PBS, 2) 20 μg of DARP-LoPE in 100 μL of PBS, 3) 1 mg of PLGA*$Z_{HER2:342}$ particles in 100 μL of PBS, and 4) 20 μg of DARP-LoPE in 100 μL of PBS and 1 mg of PLGA*$Z_{HER2:342}$ in 100 μL of PBS particles.

At the end of the treatment, all the groups were analyzed by immunohistochemistry (**Fig. S11**) with Herceptest™ (Dako) that evaluates the HER2 expression level in xenograft tumors. We found that after such a treatment of both the control and the experimental groups, the expression of HER2 is still 3+ (that means overexpression), thus making possible the application of a repeated course of therapy if necessary. The primary tumor volume was measured with a caliper and calculated using the formula $V=0.52AB^2$ (A is the largest diameter and B is the smallest diameter). The tumor growth dynamics under such treatments are shown in **Fig. 6b**. One can see that the combination of the two targeting compounds was much more efficient for *in vivo* therapy than the application of single targeting components.

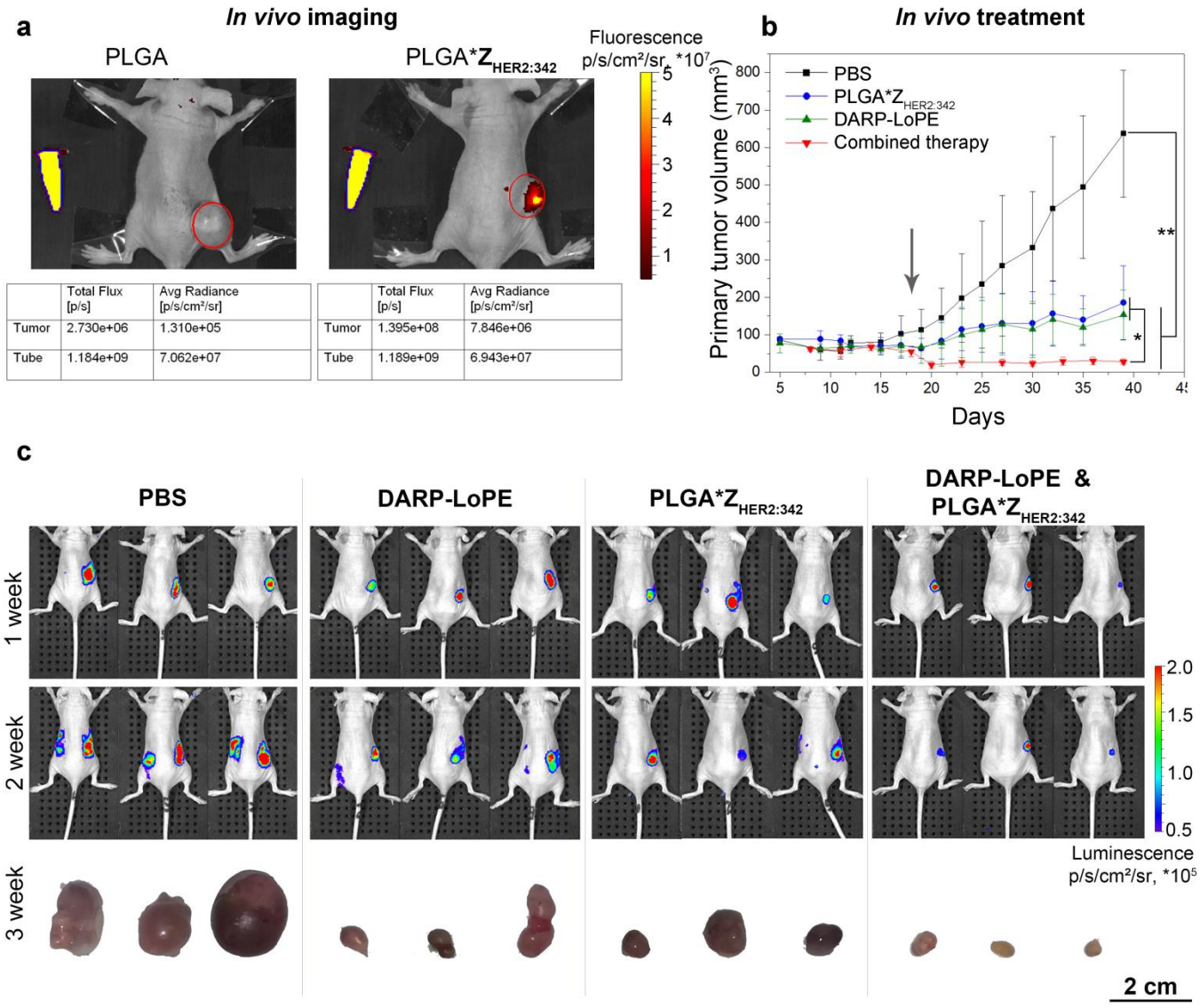

Figure 6. *HER2-positive tumor imaging and therapy in vivo.* ***a,*** *Living animal photos confirming specific labeling of HER2–overexpressing cells in vivo with PLGA*Z$_{HER2:342}$ nanoparticles. Data supported with a quantitative analysis of tumor area, expressed both as total photons flux and average radiance from selected areas (the tumor area is shown by a red circle, 0.2 mL tube with 0.05 g/L PLGA nanoparticles is shown by a blue contour).* ***b,*** *Tumor growth dynamics under treatment with PBS, PLGA*Z$_{HER2:342}$ particles alone, DARP-LoPE alone, and a combination of PLGA*Z$_{HER2:342}$ and DARP-LoPE (n=5 for each group).* ***c,*** *Imaging of BT474-NanoLuc tumor xenografts after 1 week, 2 weeks or 3 weeks after the beginning of the treatment. BALB/c Nude mice were injected with 7 µg of furimazine, and bioluminescence was recorded with IVIS Spectrum CT (Perkin Elmer).*

For the visualization of the primary tumor and metastatic sites, we made an injection of NanoLuc substrate furimazine and then imaged mice using an IVIS Spectrum CT system (Perkin Elmer). Imaging was carried out 1 week and 2 weeks after the treatment was started. As shown in **Fig. 6c**, secondary tumor nodes grew in the area of the symmetric lymph node for control (non-treated) group. For mice treated with PLGA*$Z_{HER2:342}$ or DARP-LoPE, we observed a significant reduction of the primary tumor size, but the luminescent signal was still visible on the opposite side (**Fig. 6c**). However, as the main result of this study, the group treated with a combination of PLGA*$Z_{HER2:342}$ and DARP-LoPE demonstrated a drastically reduced primary tumor size and no visual signs of secondary nodes formation during the second week after the treatment started, suggesting a high efficiency of such combination therapy for *in vivo* tumor treatment. In the third week, mice were sacrificed, and tumors were excised and imaged with a phone camera. **Fig. 6c** clearly illustrates a considerable reduction of the primary tumor volume after the application of our combination dual targeting treatment strategy.

Perspectives

Nanobiomedical engineering, which implements targeted multifunctional theranostic nanoparticles, is expected to produce major advances in early detection and treatment of cancer.[9,10,46] Nanoparticles can serve as markers for cancer imaging and sensitizers of therapies under external stimuli (such as magnetic field, light, ultrasonic, *etc*.), as well as drug carriers for chemotherapeutic agents[13,47,48] or radionuclides[49]). A major advantage of using nanoformulations is the ability to increase significantly local drug concentrations to enhance the therapeutic effect and reduce side effects. Such a treatment looks especially appealing in the case of aggressive, chemotherapy-resistant tumors and metastasis, including ones whose growth is accompanied by the overexpression of HER2 oncomarker. The employment of biodegradable nanoparticles such

as PLGA (or silicon, phosphorous, protein-based materials, *etc*.) looks especially promising for these tasks.[9,50] However, such nanoparticle-mediated therapies require the development of targeting molecules and efficient strategies of their conjugation with nanoformulations and selective delivery to cancer cells.

Conventional active targeting implies the use of full size IgG antibodies,[47,48,51] but such large molecules (150 kDa) contain not only the binding domain, but also the effector Fc part, which may significantly affect the immune response of the organism after conjugation with a nanoparticle, and thus substantially hinder the clinical translation potential of such complexes. To minimize the size of the recognizing molecule on the nanoparticle surface, single-chain variable fragments of antibody (scFv) are used,[52,53] but such an approach leads typically to a significant reduction of targeting efficiency. In particular, for anti-HER2 scFv modified PLGA nanoparticles, the uptake was only 2-fold[52] or 3-fold[53] higher for HER2-positive cells compared to HER2-negative ones. Additionally, we recently showed that direct conjugation of scFv to the nanoparticle surface is quite inefficient, leading to denaturation of the targeting molecule and the loss of its functional activity.[54,55] The recent emergence of protein-based DARPin[20,21] and affibody[22,23] molecules gives a promise for a drastic advancement of targeting strategies for nanoparticle-based theranostics. Indeed, in addition to much smaller sizes (14-18 kDa and 6–8 kDa, respectively), these molecules exhibit high affinity, low immunogenicity, excellent solubility, and stability with both N- and C-terms available for chemical conjugation and genetic engineering manipulations.

In this study, we present a synergistic targeting strategy for nanoparticle-mediated image-guided therapy based on affibody and DARPin molecules, which makes possible an improvement of efficiency of treatment of HER2-positive cancer cells. First, we demonstrated an efficient conjugation of theranostic PLGA nanoparticles with affibody $Z_{HER2:342}$ molecules and showed that

such a complex exhibited very high efficiency in labeling HER2 overexpressing cancer cells, with recorded 81-fold and 60-fold specificity *in vitro* and *in vivo*, respectively. Note that these values are more than one order of magnitude better than the specificity of PLGA particles conjugated with truncated antibody formats.[52,53] Such a high efficiency of nanoparticle targeting illustrates the preservation of the intrinsic affibody $Z_{HER2:342}$ functional activity when conjugated to the nanoparticle surface. We believe that such targeting efficiency *in vivo* can become a crucial factor for successful tumor treatment. Second, we applied recently designed targeted immunotoxin DARP-LoPE consisting of DARPin9.29 (14 kDa) and low-immunogenic fragment of Pseudomonas exotoxin A (LoPE) for the treatment of HER2-overexpressing solid tumor xenografts.

However, as the main result of this study, we demonstrated a dual targeting based therapy, which implies a simultaneous use of targeted PLGA nanoparticles and targeted immunotoxin DARP-LoPE, directed toward one molecular target: the HER2 receptor. As follows from our study, such a strategy can provide ahigh level of therapeutic efficiency with demonstrated very strong synergism of these substances. In particular, *in vitro* tests showed that the working concentration of DARP-LoPE[37] can be reduced up to 1000 times for nearly 100% cell death as revealed by the clonogenic viability assay. Moreover, the dual targeting strategy significantly improved the effectiveness of anticancer therapy *in vivo* of HER2-positive tumors, compared to monotherapy, and prevented the appearance of secondary tumor nodes.

It should be noted that this strategy is especially appealing in cases in which only one molecular target is expressed, and there is no way to improve targeted therapy by vectoring multiple receptors. To avoid metastasis and rapid mutation of tumor cells, one has to apply strategies for prompt and aggressive elimination of undesirable cells, preferably *via* different mechanisms to

initiate cell death, to achieve a higher likelihood of remission. Here, we showed that the use of two antigenic determinants of one receptor allows one to simultaneously affect cancer cells, which are capable of overexpressing only one receptor by different therapeutic modalities. It should be noted that the use of small scaffold proteins is a crucial factor in our study, as it makes possible the avoidance of steric hindrance in simultaneous targeting of a single oncomarker as it often takes place in the case of full-sized IgGs. It is also important that the proposed dual targeting-based therapy is implemented with two biocompatible and biodegradable structures, namely a protein and a biocompatible polymer, which makes this strategy very attractive for rapid translation into clinical practice. Furthermore, since the used theranostic agents have different origins and are different in size, they are excreted from the organism *via* different metabolic pathways and organs (liver/spleen for nanoparticles and kidneys for scaffolds). Thus, by combining therapeutic agents and decreasing their concentration, one can achieve the minimization of impact on organs and drastic reduction of side effects, which is very important for the development of effective strategies of oncotheranostics.

Conclusion

We demonstrated a synergistic strategy of dual regioselective targeting, implying vectoring of two distinct binding sites of the single HER2 oncomarker, with theranostic compounds, each having a different mechanism of action:

(i) *Chemotherapy agent*. Theranostic PLGA nanoformulation, loaded with an imaging diagnostic fluorescent dye (Nile Red) and a chemotherapeutic drug (doxorubicin), and functionalized with affibody $Z_{HER2:342}$;

(ii) *Immunotherapy agent.* Bifunctional genetically engineered DARP-LoPE immunotoxin comprising of a therapeutic Pseudomonas exotoxin A (LoPE) and a scaffold targeting protein, DARPin9.29.

According to the strategy, the first chemotherapy nanoagent was targeted by the affibody to subdomain III and IV of HER2 oncomarker, while the second immunotoxin is targeted by DARPin molecule to a subdomain I of HER2. By applying such synergistic dual targeting strategy, we demonstrated:

1) Significant enhancement of anticancer therapy towards HER2-overexpressing cancer cells with up to 100% cell death;
2) 1000-fold reduction of the effective concentration of targeted immunotoxin DARP-LoPE to achieve the same therapeutic effect;
3) Enhancement of the effectiveness of anticancer therapy of HER2-positive cells *in vivo* compared to monotherapies and the prevention of the appearance of secondary tumor nodes.

We believe that the strategy of dual targeting, implying "two agents – one receptor" can help to develop effective image-guided cancer therapies of aggressive tumors. We also imagine that this strategy can be extended to other combined therapies and oncotargets, including other receptors of the EGFR family, molecules of cellular adhesion, and other transmembrane receptors. Providing efficient delivery of therapeutic agents into the tumor area, the dual targeting technology renders possible a significant reduction of effective drug concentration to achieve the same effect. It is expected that such a reduction of drug dose will minimize side effects, which can be very severe under the application of non-specific chemotherapy drugs limiting the choice of subsequent treatment plans. On the other hand, the use of biocompatible nanoarchitectures and synthetic non-

immunogenic scaffold proteins for targeting leads to a very low immune response of the organism, which enables one to repeat the therapy course in the case of necessity. Furthermore, the proposed technology offers a pathway for high-efficiency treatment during a very short period of time, which is very important to avoid metastases in rapidly developing neoplasms. We believe that this oncotheranostic strategy based on dual targeting the same receptor by scaffold proteins will promote the development of efficient tools for personalized medicine.

Materials and Methods

Nanoparticle synthesis

To synthesize PLGA nanoparticles, we modified the "water-in-oil-in-water" double emulsion method described in our earlier study.[56] The synthesis methodology is schematically illustrated in **Fig. 7a**. The first emulsion was formed by the addition of 150 μL of doxorubicin hydrochloride at 2 g/L in water to 300 μL of 40 g/L PLGA (lactide: glycolide 50:50, acid and hydroxy-terminated, 25 kDa, Sigma, Germany) and 0.016 g/L Nile Red in chloroform and sonication for 1 min at 40% amplitude and for 1 min at 60% amplitude using a 130 Watt Sonicator Vibra-Cell (Sonics) at +4 ºC. The second emulsion was formed by dropping the first emulsion into 3 mL of 5% PVA (Mowiol® 4-88, Sigma, Germany) in Milli-Q water supplemented with 1 g/L of chitosan oligosaccharide lactate (5 kDa, Sigma, Germany). The solution was sonicated for 1 min at 40% amplitude and for 1 min at 60% amplitude at +4 ºC, shaken for 3 h at RT for chloroform evaporation, washed by triple centrifugation with Milli-Q water and finally resuspended in 300 μL Milli-Q water. The final concentration of the particles was determined by drying at 60 ºC.

After the chloroform evaporation and washing steps, the PLGA nanoparticles containing Dox and Nile Red with chitosan adsorbed on the surface as a corona were obtained. The cytotoxic agent Dox was included in the first "water" phase; the imaging dye Nile Red was incorporated into the "oil" phase together with PLGA. Synthesized PLGA particles exhibited both –COOH and $–NH_2$ chemical groups on the surface, which made possible their direct chemical conjugation to proteins, namely, affibody $Z_{HER2:342}$.

Finally, to specifically target the synthesized nanoparticles **(Fig. 7b)** to HER2 positive cells, we attached a HER2–recognizing affibody, namely, $Z_{HER2:342}$, to the surface of the nanoparticles using carbodiimide chemistry (**Fig. 7c**).

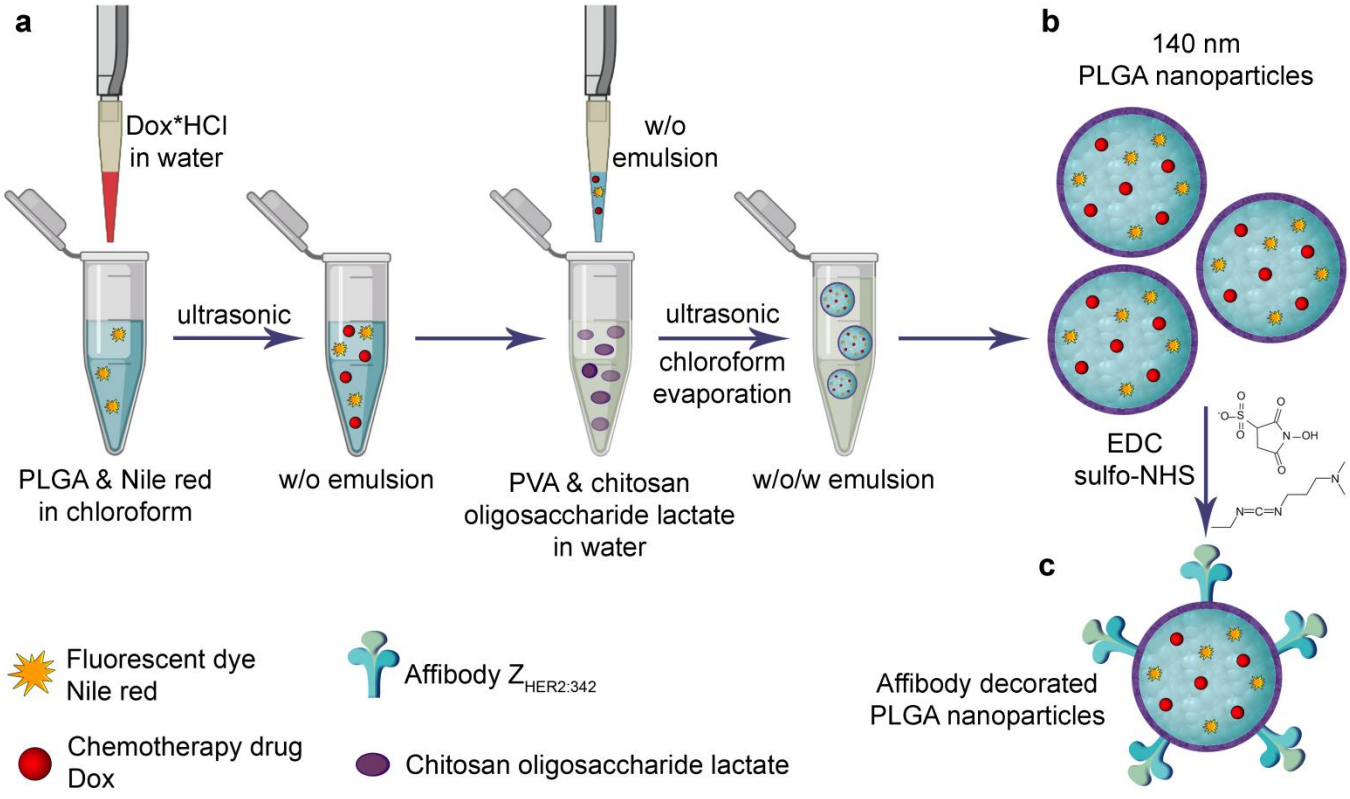

Figure 7. *Scheme of PLGA nanoparticles synthesis.* ***a****, Synthesis of PLGA nanoparticles by double water-oil-water emulsion method.* ***b****, Schematic representation of PLGA nanoparticles loaded with*

Nile Red (diagnostic) and doxorubicin (therapeutic). ***c,*** *Modification of PLGA nanoparticles with affibody* $Z_{HER2:342}$ *by carbodiimide chemistry.*

Doxorubicin loading measurement

PLGA nanoparticles were synthesized as described above excluding the addition of Nile Red to prevent Nile Red fluorescence interference with the doxorubicin fluorescent signal. 1 mg of PLGA nanoparticles was dissolved in the mixture water:DMSO 50:50 for 1 h at 37 °C. Fluorescence of the solution was measured using an Infinite M100 Pro (Tecan, Austria) microplate reader at an excitation wavelength of 482 nm and an emission wavelength of 584 nm. Using the fluorescence-concentration calibration curve for free Dox in the same solution, the Dox content in PLGA was measured.

Doxorubicin release measurement

PLGA nanoparticles were synthesized as described above, excluding the addition of Nile Red to prevent Nile Red fluorescence interference with doxorubicin fluorescent signal. PLGA nanoparticles at 1g/L were placed in buffers with different pH: pH 2 (0.1 M glycine-HCl), pH 3 (0.1 M glycine-HCl), pH 4 (0.1 M citrate buffer), pH 5 (0.15 M citrate-phosphate buffer), pH 6 (0.1 M HEPES buffer), pH 7 (0.15 M phosphate buffer). 1 min, 20 min, 1 h, 4 h, 20 h, 30 h later 100μL-aliquots were taken, centrifuged for 5 min at 10000g, and the fluorescence of the samples was measured. All samples were analyzed in triplicates. For each buffer solution, a concentration-fluorescence calibration curve was made (since Dox fluorescence strongly depends on pH). The released portion of doxorubicin was then measured and presented as % from total Dox content in the PLGA nanoparticle sample.

Electron microscopy

Scanning electron microscopy images of PLGA nanoparticles were obtained with a MAIA3 electron microscope (Tescan, Czech Republic) at an accelerating voltage of 5 kV. The samples were deposited onto a silicon wafer and then air-dried at the ambient conditions. SEM images were evaluated using ImageJ software to get a particle size distribution.

Fluorescence spectroscopy

PLGA nanoparticle excitation and emission spectra were acquired using a Infinite M100 Pro (Tecan, Austria) microplate reader. The nanoparticle suspension in 100 μL of PBS at a concentration of 10 μg/mL was placed into 96 flat-bottomed plate. The excitation spectrum was recorded within the range of 350 – 650 nm (emission wavelength was 670 nm) at bottom mode with a gain of 145 and an integration time of 20 μs. The emission spectrum was recorded within the range of 510 – 850 nm (excitation wavelength was 490 nm) at bottom fluorescence mode with a gain of 168 and an integration time of 20 μs.

Dynamic and electrophoretic light scattering measurements

Hydrodynamic sizes of nanoparticles were determined using a Zetasizer Nano ZS (Malvern Instruments Ltd, UK) analyzer in PBS buffer (137 mM NaCl, 2.7 mM KCl, 4.77 mM Na_2HPO_4, 1.7 mM KH_2PO_4, pH 7.4) at 25 °C. All measurements were performed in triplicates. Z-potentials of the nanoparticles were determined using the Zetasizer Nano ZS (Malvern Instruments Ltd, UK) analyzer in 10 mM KNO_3 buffer at 25 °C. All measurements were performed in triplicate.

Affibody $Z_{HER2:342}$ and DARP-LoPE isolation and purification

Protein production. Affibody $Z_{HER2:342}$ was produced in *Escherichia coli* strain BL21(DE3) (Novagen-EMD Millipore, Madison, WI 53719, USA).

The $Z_{HER2:342}$ gene nucleotide sequence was deduced from a $Z_{HER2:342}$ amino acid sequence,[32] taking into account the codon usage in highly expressed *E. coli* genes with the help of freely distributed software DNABuilder (http://www.innovationsinmedicine.org/software/DNABuilder/).

The gene was assembled by PCR from chemically synthesized oligonucleotides of 50 bp in length having partially complementary sequences. PCR reactions were performed using a thermostable polymerase Tersus (Evrogen, Moscow, Russia, www.evrogen.ru) in conditions recommended by the supplier. The amino acid sequence encoded by the $Z_{HER2:342}$ gene was as follows: MRGSHHHHHHGSVDNKFNKEMRNAYWEIALLPNLNNQQKRAFIRSLYDDPSQSANLL AEAKKLNDAQAPK. The gene was cloned into the plasmid vector pET39b (Novagen-EMD Millipore, Madison, WI 53719, USA) between restriction sites NdeI and HindIII. The resultant plasmid was called as pET39-Z342. The expression cassette was sequence verified by Evrogen (Russia). *E. coli*, transformed with pET39-Z342, was grown in autoinduction ZYM-5052 medium[57] containing 100 μg/mL kanamycin at 25 ºC. The cells were harvested by centrifugation at 10,000 g at 4 ºC for 20 min and resuspended in lysis buffer (200 mM Tris-HCl, 500 mM sucrose, 1 mM EDTA (pH 8.0), 1 mM PMSF and 60 μg/mL lysozyme). The suspension was diluted two-fold with distilled water and incubated at room temperature for 30 min. Cells were broken on ice using a Vibra Cell ultrasonic liquid processor VCX130 (Sonics & Materials, Inc., Newtown, CT, USA). The cellular debris was pelleted at 70,000 g at 4 ºC for 30 min. After the addition of imidazole (30 mM) and NaCl (500 mM), the supernatant was filtered through a 0.22 μm membrane and applied onto a HisTrap HP, 1 mL column (GE Healthcare) equilibrated with 20 mM sodium phosphate buffer (pH 7.5), 500 mM NaCl and 30 mM imidazole. The bound proteins were eluted

with a linear 30-500 mM imidazole gradient. The fractions were analyzed by 15% reducing SDS-PAGE. Protein concentration was determined by UV spectroscopy using ε280 = 8 250 $M^{-1}cm^{-1}$.

DARP-LoPE protein was purified as previously described with the following modifications. E. coli BL21(DE3) were transformed with previously obtained plasmid pDARP-LoPE[36]. Freshly grown transformed cells were inoculated into medium containing 2 mM $MgSO_4$, 25 mM Na_2HPO_4, 25 mM KH_2PO_4, 50 mM NH_4Cl, 5 mM Na_2SO_4, 1% yeast extract, 2% tryptone, and 0.2 g/L ampicillin and grown until OD_{600} = 0.5 was reached. Then, IPTG was added, and cells were grown under intense aeration for 24 h at 20 °C. Next, the cells were harvested by centrifugation at 5000 g and 4 °C for 15 min. Then, the precipitate was resuspended in lysing buffer (20 mM Na-Pi, 500 mM NaCl, pH 7.5, 50 μg/mL lysozyme) and destroyed by applying ultrasound. Cell debris was removed by centrifugation at 20000 g for 60 min at 4 °C. The lysate was then filtered and applied onto a Ni^{2+}-NTA column (GE Healthcare, USA) in buffer containing 20 mM NaPi, pH 7.4, 500 mM NaCl, and 30 mM imidazole, and protein was eluted with imidazole step gradient (50, 100, 150, 200, 250, and 500 mM).

PLGA conjugation with $Z_{HER2:342}$

Covalent modification of PLGA nanoparticles with affibody $Z_{HER2:342}$ molecules was achieved using sodium salt of 1-ethyl-3-(3-dimethyl aminopropyl) carbodiimide (EDC, Sigma, Germany) and the sodium salt of N-hydroxysulfosuccinimide (sulfo-NHS, Sigma, Germany) as crosslinking agents *via* the formation of amide bonds between the carboxyl groups on the particle surface and protein amino groups. 1 mg of PLGA nanoparticles in 200 μL of 0.1 M 2-(N-morpholino) ethanesulfonic acid buffer, pH 5.5 were activated with 20 mg EDC and 10 mg sulfo-NHS for 15 min at 20 °C. The excess of unreacted reagents were removed by centrifugation for 5 min at 5000

g. Next, 150 μg of affibody $Z_{HER2:342}$ and 200 μg of BSA were quickly added to activated PLGA nanoparticles in 200 μL of borate buffer (0.4 M H_3BO_3, 70 mM $Na_2B_4O_7$, pH 8.0) and sonicated for several seconds. The reaction was carried overnight at RT, followed by particle washing from non-bound proteins by triple centrifugation at 10000 g for 10 min.

The quantity of conjugated proteins on the surface of PLGA nanoparticles was determined by the BCA Protein Assay (Pierce, USA). PLGA particles were conjugated to proteins, as described above, in 1.5 mL Eppendorf LoBind Protein microcentrifuge tubes. The control Eppendorf 1.5 mL tubes with the same buffers and crosslinkers were used as a control. After the conjugation procedure, particles and control tubes were centrifuged under the same conditions and the protein content in the supernatant was measured using the BCA assay according to manufacturer recommendations using the calibration curve. The difference in protein content between the test and control tubes were considered as the quantity of protein conjugated to PLGA particles.

Protein conjugation to FITC and Cy5.5

FITC-labeled $Z_{HER2:342}$ and DARP-LoPE were prepared as follows. 100 μg of $Z_{HER2:342}$ or DARP-LoPE in 90 μL of PBS buffer was rapidly mixed with 10 μL FITC in DMSO at concentrations of 7 g/L and 1.4 g/L, respectively. Proteins were incubated overnight at RT and purified from unreacted FITC molecules using Zeba Spin Desalting Columns, 7k MWCO (Pierce, USA) according to manufacturer's recommendations. FITC-labeled Trastuzumab was prepared as described by us previously.[58]

DARP-LoPE*Cy5.5 was prepared as follows. 100 μg of DARP-LoPE in 90 μL of 0.5 M NaCl was rapidly mixed with 10 μL sulfo-Cyanine5.5 NHS ester (Lumiprobe, Russia) in the water at concentrations of 2 g/L. Incubation was performed 4 h at RT and protein was purified from

unreacted molecules using Zeba Spin Desalting Columns according to manufacturer's recommendations.

Cell culture

Cell lines of human breast adenocarcinoma SK-BR-3 (HTB-30™; ATCC), ductal carcinoma BT-474 (HTB-20™; ATCC), lung carcinoma A549 (CCL-185™; ATCC) and Chinese hamster ovary CHO (Russian Cell Culture Collection) were maintained in DMEM medium (HyClone, USA) supplemented with 10% fetal bovine serum (HyClone, USA) and 2 mM L-glutamine (PanEko, Russia). Cells were incubated under a humidified atmosphere with 5% CO_2 at 37 °C.

To obtain a stable BT/NanoLuc cell line, a plasmid encoding NanoLuc luciferase gene was constructed based on our previously described constructs.[59,60] NanoLuc gene was under the control of the CMV promoter, and plasmid contained the puromycin resistance gene under NP promoter. For transfections, plasmid DNA isolated from bacterial cells with the PureLinkTM kit (Invitrogen) was used according to the manufacturer's instructions. Transfection of BT-474 cells was performed using FuGENE® HD (Promega) according to the manufacturer's recommendations (http://www.promega.com/techserv/tools/FugeneHdTool/). A day before the transfection, the cells were seeded at a density of 10^5 cells/mL in a complete growth medium without antibiotics. FuGENE® HD and DNA were used in a 3:1 ratio, and the concentration of the plasmid DNA during the formation of the complexes was 0.02 μg/μL. The volume of the medium that was added to the cells and contained FuGENE® HD–DNA complexes was 1/20 of the total volume of the growth medium. The complexes were prepared in a medium without serum and antibiotics, cultured at room temperature for 5–10 min and added to the cells. The concentration of puromycin (Sigma, Germany) that caused the death of 100% of the cells for 14 days (2 μg/mL for BT-474

cells) was detected during preliminary experiments. The medium was replaced with a fresh medium containing puromycin 24 h after transfection. Clones of the stably transfected cells were formed by day 14–15, after which the cells were passaged in the presence of puromycin at the maintaining concentration of puromycin (1 μg/mL).

Flow cytometry

To determine $Z_{HER2:342}$-FITC and PLGA*$Z_{HER2:342}$ specificities, the harvested cells were washed with PBS, resuspended in 300 μL of PBS with 1% BSA at a concentration of 10^6 cells per mL, labeled with $Z_{HER2:342}$-FITC at a final concentration of 2 μg/mL or PLGA nanoparticles at 0.1 g/L, washed and analyzed using Novocyte 3000 VYB flow cytometer (ACEA Biosciences, USA) in BL1 channel (excitation laser 488 nm, emission filter 530/30 nm) for $Z_{HER2:342}$-FITC and in YL2 channel (excitation laser 561 nm, emission filter 615/20 nm) for PLGA nanoparticles.

To evaluate DNA content in cell cycle phases, cells were analyzed with the BD Accuri C6 flow cytometer (BD, USA) in FL2 channel (excitation laser 488 nm, emission filter 585/40 nm), followed with data analysis with CFlow Plus and FlowJo software.

Confocal laser scanning microscopy

To visualize PLGA nanoparticles by confocal laser scanning microscopy, cells were incubated with 30 μg/mL of PLGA nanoparticles and Hoechst 33342 (1 μg/mL) on ice for 30 min in PBS with 1% BSA, washed from unbound nanoparticles, and then incubated for 15 min at +37 ºC, followed by confocal laser scanning microscopy imaging using a Leica DMI6000B system (Leica Microsystems, Germany) microscope equipped with Confocal Microscopy Upgrade (Thorlabs, USA) at the following conditions: Hoechst 33342: excitation laser – 405 nm, emission filter –

440/40 nm; PLGA: excitation laser – 561 nm, emission filter – 600/52 nm. For DARP-LoPE visualization study cells were labeled with 5 μg/mL DARP-LoPE and Hoechst 33342 (1 μg/mL) on ice for 30 min in PBS with 1% BSA, washed from unbound molecules and imaged at the following conditions: Hoechst 33342: excitation laser – 405 nm, emission filter – 440/40 nm; FITC: excitation laser – 488 nm, emission filter – 525/45 nm.

To study the intracellular trafficking of PLGA*$Z_{HER2:342}$ nanoparticles, cell endosomes were labeled with GFP 48 h prior to transfection with CellLight Early Endosomes-GFP BacMam 2.0 (Invitrogen, USA) according to manufacturer recommendations. Cell lysosomes were labeled with LysoTracker DeepRed (Invitrogen, USA) 30 min before cell labeling according to manufacturer recommendations. Cells were incubated with 30 μg/mL of PLGA and imaged under the following conditions: GFP-endosomes: excitation laser 488 nm, emission filter 440/40 nm; PLGA: excitation laser 561 nm, emission filter 600/52 nm; lysosomes: excitation laser 642 nm, emission filter 647LP nm; nuclei stained with Hoechst 33342: excitation laser 405 nm, emission filter 440/40 nm".

DNA content evaluation

Cells were seeded at 12-well flat-bottomed culture plates, incubated overnight under a humidified atmosphere with 5% CO_2 at 37 °C in DMEM growth medium. Next, PLGA or PLGA*$Z_{HER2:342}$ nanoparticles were added to wells at different concentrations, and cells were incubated overnight. Next, cells were harvested from culture plate with 2 mM EDTA solution, centrifuged for 5 min at 100 g, and 700 μL of ice-cold 70% ethanol was added to each tube. Cells were incubated for 1 h at +4 ºC and centrifuged for 10 min at 1000 g. Next, 200 μL of propidium iodide at 50 μg/mL and RNAse A at 0.05 g/L were added to cells. Samples were incubated for 15 min at RT and analyzed with flow cytometry.

MTT assay

Cytotoxicity of synthesized targeted and non-targeted nanoparticles, as well as that of immunotoxin DARP-LoPE, was investigated using a standard MTT assay. Cells were seeded on a 96-well plate at 10^4 cells per well in 100 μL of DMEM medium supplemented with 10% FBS and cultured overnight. Nanoparticles and proteins under investigation were added to wells in 100 μL of DMEM growth medium, and cells were incubated for 48 h or 72 h. Then the medium was removed, and 100 μL of MTT solution (0.5 g/L in DMEM) was added to the cells. Samples were incubated for 2 hours at 37 °C, MTT solution was then removed, and 100 μL of DMSO was added to the wells. The plate was gently shaken until the formazan crystals dissolved completely. The optical density of each well was measured using Infinite 1000 Pro (Tecan, Austria) microplate reader at a wavelength of λ = 570 nm. The IC50 value was determined by GraphPad Prism software.

Clonogenic assay

10^5 cells were incubated with targeted and non-targeted nanoparticles as well as with immunotoxin DARP-LoPE in DMEM growth medium for a short time (30 min) at +37 ºC. The cells were diluted 100 times with DMEM growth medium, 1000 cells were seeded for 1 well of 12-well flat-bottomed culture plates and cultured for 3 weeks. Then, the culture medium was decanted, cells were washed with 500 μL of PBS:methanol 50:50 mixture, then fixed with methanol for 1 h at RT, and stained with 1% crystal violet for 15 min at RT. The cells were then washed 10-times with water, followed by visual counting of grown cell colonies. The results (number of cell colonies) were presented depending on the initial concentration of targeted compounds before the dilution.

Real-time cell analysis

E16 xCELLigence plates were prepared by the addition of complete cell culture media (50 μL) to every well. After equilibration to 37 °C, the plates were inserted into an xCELLigence station, and the cell index was measured to get a baseline and to ensure that all wells and connections were in operation within acceptable limits. Then, 4000 SK-BR-3 cells in 50 μL of complete cell culture media were added to wells and were allowed to attach for 24 h. Then, PLGA particles were added at three different concentrations and kinetics of binding and cell growth were measured for three days.

Tumor-bearing mice

Female BALB/c Nude mice were purchased from Puschino Animal Facility and maintained at Vivarium of Institute of Bioorganic Chemistry (IBCh RAS). All procedures were approved by the IBCh RAS Institutional Animal Care and Use Committee. Female BALB/c Nude mice (22 – 25 g) were inoculated subcutaneously with $2 \cdot 10^6$ BT/NanoLuc HER2 overexpressing cancer cells in 30% Matrigel in culture medium. The level of *in vivo* HER2 receptor expression was confirmed using flow cytometry (see **Fig. S7** and **Note S2**).

Living animal imaging and visualization of PLGA particles

When tumor volume reached 600 mm^3, mice received intravenously 150 μg of JO-4 protein (to trigger the transient opening of intercellular junctions in tumor[61]) into the right retroorbital sinus. Then, 1 hour later 1.5 mg of PLGA or PLGA*$Z_{HER2:342}$ nanoparticles were injected into the left retro-orbital sinus. 2 hours later mice were anesthetized with a mixture of Tiletamine-HCl / Zolazepam-HCl / Xylazine-HCl in a dose of 20/20/1.6 mg/kg and visualized with IVIS Spectrum CT imaging system (Perkin Elmer, USA).

Living animal were visualized using the IVIS Spectrum CT imaging system (Perkin Elmer, USA) with the following excitation filters: 465, 500, 535, and 570 nm and emission filters: 520, 540, 560, 580, 600, 620, 640, and 660 nm, followed by Living Image software processing and autofluorescence subtraction using a Living Image Spectral Unmixing Tool. As a control of uniform settings for all acquired images, a tube containing 0.05 g/L PLGA nanoparticles was imaged along with the animals.

In vivo tumor therapy with DARP-LoPE and PLGA*$Z_{HER2:342}$

After tumor inoculation (day 0) at day 18, mice were randomly divided into 4 groups (n=5 or n=6). The first group (control) received a daily 100 µL of PBS solution intravenously in the retroorbital sinus. Mice from the second group were treated every day with 20 µg of DARP-LoPE in 100 µL of PBS for 9 days (a total of 5 injections of 20 µg of DARP-LoPE) by intravenous injection in the retroorbital sinus. The third group received every day 150 µg of JO-4 protein into the right retroorbital sinus and then 1 hour later 1 mg of PLGA*$Z_{HER2:342}$ in 100 µL into the left retroorbital sinus for 9 days (a total of 5 injections of 1 mg of PLGA*$Z_{HER2:342}$). Mice from the fourth group received sequentially daily alternating injections of DARP-LoPE and PLGA*$Z_{HER2:342}$ particles (a total of 5 injections of 150 µg of JO-4 protein and 1 mg of PLGA*$Z_{HER2:342}$ and 5 injections of 20 µg of DARP-LoPE per mouse).

One and two weeks after treatment start, tumors were visualized with the IVIS Spectrum CT imaging system (Perkin Elmer, USA). Mice received 3.5 µL of furimazine in 100 µL of PBS by intraperitoneal injection, and after 20 min, tumor bioluminescence mice were visualized with an open filter on IVIS Spectrum CT. 3 weeks after the start of treatment, mice were sacrificed, and tumors were isolated and visualized with a smartphone camera.

Supporting Information

The Supporting Information is available free of charge at https://pubs.acs.org/doi/xx.xxxx/acsnano.xxxxxxx.

Particle characterization, flow cytometry results, and gating strategy, doxorubicin toxicity study by MTT-test, chromosomal DNA fragmentation evaluation, synergy quantification, clonogenic assay results, *in vivo* tumor model evaluation, immunohistochemistry results.

Author Information

Corresponding Author

*Correspondence to Victoria Shipunova viktoriya.shipunova@phystech.edu, Andrei Kabashin kabashin@lp3.univ-mrs.fr, and Paras Prasad pnprasad@buffalo.edu

Author Contributions

The manuscript was written through the contributions of all authors. All authors have given approval to the final version of the manuscript.

Acknowledgements

The work was supported in part by the Russian Science Foundation grants № 17-74-20146 (particle synthesis and characterization, *in vivo* studies) and 19-72-30012 (electron microscopy study), and by the Russian Foundation for Basic Research grant № 20-34-70136 (theranostic immunotoxin purification) and 19-29-04012 (*in vitro* toxicity studies), by the Institute for Lasers, Photonics and Biophotonics from a fund provided by the Office of Vice President for Research

and Economic Development at the University at Buffalo, and by MEPhI Academic Excellence Project (Contract No. 02.a03.21.0005).

We thank Dr. Supriya D. Mahajan, Research Associate Professor (Department of Medicine, Division of Allergy, Immunology, and Rheumatology, State University of New York at Buffalo, Clinical Translational Research Center, Buffalo, NY, USA) for assisting with colony formation assay.

References

(1) Love, R. R.; Leventhal, H.; Easterling, D. V.; Nerenz, D. R. Side Effects and Emotional Distress during Cancer Chemotherapy. *Cancer* **1989**, *63*, 604–612.

(2) Monsuez, J.-J.; Charniot, J.-C.; Vignat, N.; Artigou, J.-Y. Cardiac Side-Effects of Cancer Chemotherapy. *Int. J. Cardiol.* **2010**, *144*, 3–15.

(3) Argyriou, A. A.; Bruna, J.; Marmiroli, P.; Cavaletti, G. Chemotherapy-Induced Peripheral Neurotoxicity (CIPN): An Update. *Crit. Rev. Oncol. Hematol.* **2012**, *82*, 51–77.

(4) Editorial. Powerful Combination Therapies. *Nat. Biomed. Eng.* **2018**, *2*, 555–556.

(5) Ghetie, M. A.; Bright, H.; Vitetta, E. S. Homodimers but Not Monomers of Rituxan (Chimeric Anti-CD20) Induce Apoptosis in Human B-lymphoma Cells and Synergize with a Chemotherapeutic Agent and an Immunotoxin. *Blood* **2001**, *97*, 1392–1398.

(6) Scadden, D. T.; Schenkein, D. P.; Bernstein, Z.; Luskey, B.; Doweiko, J.; Tulpule, A.; Levine, A. M. Immunotoxin Combined with Chemotherapy for Patients with AIDS-Related Non-Hodgkin's Lymphoma. *Cancer* **1998**, *83*, 2580–2587.

(7) Potala, S.; Sahoo, S. K.; Verma, R. S. Targeted Therapy of Cancer Using Diphtheria Toxin-Derived Immunotoxins. *Drug Discov. Today* **2008**, *13*, 807–815.

(8) Pastan, I.; Hassan, R.; Fitzgerald, D. J.; Kreitman, R. J. Immunotoxin Therapy of Cancer. *Nat. Rev. Cancer* **2006**, *6*, 559–565.

(9) Kabashin, A. V.; Singh, A.; Swihart, M. T.; Zavestovskaya, I. N.; Prasad, P. N. Laser-Processed Nanosilicon: A Multifunctional Nanomaterial for Energy and Healthcare. *ACS Nano* **2019**, *13*, 9841–9867.

(10) Prasad, P. N. *Introduction to Nanomedicine and Nanobioengineering*; Wiley Series in Biomedical Engineering and Multi-Disciplinary Integrated Systems; Wiley: Hoboken, NJ, 2012.

(11) Chen, G.; Roy, I.; Yang, C.; Prasad, P. N. Nanochemistry and Nanomedicine for Nanoparticle-Based Diagnostics and Therapy. *Chem. Rev.* **2016**, *116*, 2826–2885.

(12) Anselmo, A. C.; Mitragotri, S. Nanoparticles in the Clinic. *Bioeng. Transl. Med.* **2016**, *1*, 10–29.

(13) Zelepukin, I. V.; Yaremenko, A. V.; Shipunova, V. O.; Babenyshev, A. V.; Balalaeva, I. V.; Nikitin, P. I.; Deyev, S. M.; Nikitin, M. P. Nanoparticle-Based Drug Delivery *via* RBC-Hitchhiking for the Inhibition of Lung Metastases Growth. *Nanoscale* **2019**, *11*, 1636–1646.

(14) Nikitin, M. P.; Shipunova, V. O.; Deyev, S. M.; Nikitin, P. I. Biocomputing Based on Particle Disassembly. *Nat. Nanotechnol.* **2014**, *9*, 716–722.

(15) Tietjen, G. T.; Bracaglia, L. G.; Saltzman, W. M.; Pober, J. S. Focus on Fundamentals: Achieving Effective Nanoparticle Targeting. *Trends. Mol. Med.* **2018**, *24*, 598–606.

(16) Rijpkema, M.; Boerman, O. C.; Oyen, W. J. G. Tumor Targeting Using Radiolabeled Antibodies for Image-Guided Drug Delivery. *Curr. Drug Targets* **2015**, *16*, 625–633.

(17) Fleuren, E. D. G.; Versleijen-Jonkers, Y. M. H.; Heskamp, S.; van Herpen, C. M. L.; Oyen, W. J. G.; van der Graaf, W. T. A.; Boerman, O. C. Theranostic Applications of Antibodies in Oncology. *Mol. Oncol.* **2014**, *8*, 799–812.

(18) Heinzmann, K.; Carter, L. M.; Lewis, J. S.; Aboagye, E. O. Multiplexed Imaging for Diagnosis and Therapy. *Nat. Biomed. Eng.* **2017**, *1*, 697–713.

(19) Moek, K. L.; Giesen, D.; Kok, I. C.; Groot, D. J. A. de; Jalving, M.; Fehrmann, R. S. N.; Lub-de Hooge, M. N.; Brouwers, A. H.; Vries, E. G. E. de. Theranostics Using Antibodies and Antibody-Related Therapeutics. *J. Nucl. Med.* **2017**, *58*, 83S-90S.

(20) Boersma, Y. L.; Plückthun, A. DARPins and Other Repeat Protein Scaffolds: Advances in Engineering and Applications. *Curr. Opin. Biotech.* **2011**, *22*, 849–857.

(21) Stumpp, M. T.; Binz, H. K.; Amstutz, P. DARPins: A New Generation of Protein Therapeutics. *Drug Discov. Today* **2008**, *13*, 695–701.

(22) Nygren, P.-A. Alternative Binding Proteins: Affibody Binding Proteins Developed from a Small Three-Helix Bundle Scaffold. *FEBS J.* **2008**, *275*, 2668–2676.

(23) Löfblom, J.; Feldwisch, J.; Tolmachev, V.; Carlsson, J.; Ståhl, S.; Frejd, F. Y. Affibody Molecules: Engineered Proteins for Therapeutic, Diagnostic and Biotechnological Applications. *FEBS Lett.* **2010**, *584*, 2670–2680.

(24) Gao, J.-Q.; Lv, Q.; Li, L.-M.; Tang, X.-J.; Li, F.-Z.; Hu, Y.-L.; Han, M. Glioma Targeting and Blood–Brain Barrier Penetration by Dual-Targeting Doxorubincin Liposomes. *Biomaterials* **2013**, *34*, 5628–5639.

(25) Kontermann, R. E. Dual Targeting Strategies with Bispecific Antibodies. *mAbs* **2012**, *4*, 182–197.

(26) Regales, L.; Gong, Y.; Shen, R.; Stanchina, E. de; Vivanco, I.; Goel, A.; Koutcher, J. A.; Spassova, M.; Ouerfelli, O.; Mellinghoff, I. K.; Zakowski, M.F.; Politi, K.A.; Pao, W. Dual Targeting of EGFR Can Overcome a Major Drug Resistance Mutation in Mouse Models of EGFR Mutant Lung Cancer. *J. Clin. Invest.* **2009**, *119*, 3000–3010.

(27) Lemmon, M. A.; Schlessinger, J. Cell Signaling by Receptor Tyrosine Kinases. *Cell* **2010**, *141*, 1117–1134.

(28) Gullick, W. J. Update on HER-2 as a Target for Cancer Therapy: Alternative Strategies for Targeting the Epidermal Growth Factor System in Cancer. *Breast Cancer Res.* **2001**, *3*, 34913.

(29) Press, M. F.; Slamon, D. J.; Flom, K. J.; Park, J.; Zhou, J.-Y.; Bernstein, L. Evaluation of HER-2/neu Gene Amplification and Overexpression: Comparison of Frequently Used Assay Methods in a Molecularly Characterized Cohort of Breast Cancer Specimens. *JCO* **2002**, *20*, 3095–3105.

(30) Yan, M.; Schwaederle, M.; Arguello, D.; Millis, S. Z.; Gatalica, Z.; Kurzrock, R. HER2 Expression Status in Diverse Cancers: Review of Results from 37,992 Patients. *Cancer Metastasis Rev.* **2015**, *34*, 157–164.

(31) Nord, K.; Gunneriusson, E.; Ringdahl, J.; Ståhl, S.; Uhlén, M.; Nygren, P.-Å. Binding Proteins Selected from Combinatorial Libraries of an α-Helical Bacterial Receptor Domain. *Nat. Biotechnol.* **1997**, *15*, 772–777.

(32) Orlova, A.; Magnusson, M.; Eriksson, T. L.J.; Nilsson, M.; Larsson, B.; Höidén-Guthenberg, I.; Widström, C.; Carlsson, J.; Tolmachev, V.; Ståhl, S.; Nilsson, F.Y. Tumor Imaging Using a Picomolar Affinity HER2 Binding Affibody Molecule. *Cancer Res.* **2006**, *66*, 4339–4348.

(33) Ekerljung, L.; Lennartsson, J.; Gedda, L.; Lau, K. M. The HER2-Binding Affibody Molecule (ZHER2:342)2 Increases Radiosensitivity in SKBR-3 Cells. *PLoS ONE* **2012**, *7*, e49579.

(34) Tran, T.; Engfeldt, T.; Orlova, A.; Sandström, M.; Feldwisch, J.; Abrahmsén, L.; Wennborg, A.; Tolmachev, V.; Karlström, A. E. 99m Tc-maEEE-Z HER2:342, an Affibody Molecule-Based Tracer for the Detection of HER2 Expression in Malignant Tumors. *Bioconjugate Chem.* **2007**, *18*, 1956–1964.

(35) Baum, R. P.; Prasad, V.; Muller, D.; Schuchardt, C.; Orlova, A.; Wennborg, A.; Tolmachev, V.; Feldwisch, J. Molecular Imaging of HER2-Expressing Malignant Tumors in Breast Cancer Patients Using Synthetic 111In- or 68Ga-Labeled Affibody Molecules. *J. Nucl. Med.* **2010**, *51*, 892–897.

(36) Proshkina, G. M.; Kiseleva, D. V.; Shilova, O. N.; Ryabova, A. V.; Shramova, E. I.; Stremovskiy, O. A.; Deyev, S. M. Bifunctional Toxin DARP-LoPE Based on the Her2-Specific Innovative Module of a Non-Immunoglobulin Scaffold as a Promising Agent for Theranostics. *Mol. Biol.* **2017**, *51*, 865–873.

(37) Sokolova, E. A.; Shilova, O. N.; Kiseleva, D. V.; Schulga, A. A.; Balalaeva, I. V.; Deyev, S. M. HER2-Specific Targeted Toxin DARPin-LoPE: Immunogenicity and Antitumor Effect on Intraperitoneal Ovarian Cancer Xenograft Model. *Int. J. Mol. Sci.* **2019**, *20*.

(38) Jost, C.; Schilling, J.; Tamaskovic, R.; Schwill, M.; Honegger, A.; Plückthun, A. Structural Basis for Eliciting a Cytotoxic Effect in HER2-Overexpressing Cancer Cells *via* Binding to the Extracellular Domain of HER2. *Structure* **2013**, *21*, 1979–1991.

(39) Kefayat, A.; Vaezifar, S. Biodegradable PLGA Implants Containing Doxorubicin-Loaded Chitosan Nanoparticles for Treatment of Breast Tumor-Bearing Mice. *Int. J. Biol. Macromol.* **2019**, *136*, 48–56.

(40) Coyne, C. P.; Ross, M. K.; Bailey, J. G. Dual Potency Anti-HER2/neu and Anti-EGFR Anthracycline Immunoconjugates in Chemotherapeutic-Resistant Mammary Carcinoma Combined with Cyclosporin A and Verapamil P-Glycoprotein Inhibition. *J. Drug Target.* **2009**, 17, 474–489.

(41) Chou, T.-C. Theoretical Basis, Experimental Design, and Computerized Simulation of Synergism and Antagonism in Drug Combination Studies. *Pharmacol. Rev.* **2006**, *58*, 621–681.

(42) Chou, T.-C. Drug Combination Studies and Their Synergy Quantification Using the Chou-Talalay Method. *Cancer Res.* **2010**, *70*, 440–446.

(43) Riss, T. L.; Moravec, R. A.; Niles, A. L.; Duellman, S.; Benink, H. A.; Worzella, T. J.; Minor, L. Cell Viability Assays. In *Assay Guidance Manual [Internet]*; Sittampalam, G. S., Grossman,

A., Brimacombe, K., *et al.*, Eds.; Eli Lilly & Company and The National Center for Advancing Translational Sciences: Bethesda (MD), 2016, pp 1−59.

(44) O'Hare, S.; Atterwill, C. K. *In Vitro Toxicity Testing Protocols*; Humana Press: Totowa, NJ, 1995.

(45) Stoddart, M. J. *Mammalian Cell Viability: Methods and Protocols*; Springer protocols 740; Springer: New York, 2011, pp 13-19.

(46) He, G. S.; Tan, L.-S.; Zheng, Q.; Prasad, P. N. Multiphoton Absorbing Materials: Molecular Designs, Characterizations, and Applications. *Chem. Rev.* **2008**, *108*, 1245–1330.

(47) Sun, B. F.; Feng, S. S. Trastuzumab Decorated Nanoparticles for Targeted Chemotherapy of Breast Cancer. *AST* **2008**, *57*, 160–165.

(48) Sun, B.; Ranganathan, B.; Feng, S.-S. Multifunctional Poly(d,l-Lactide-Co-Glycolide)/Montmorillonite (PLGA/MMT) Nanoparticles Decorated by Trastuzumab for Targeted Chemotherapy of Breast Cancer. *Biomaterials* **2008**, *29*, 475–486.

(49) Petriev, V. M.; Tischenko, V. K.; Mikhailovskaya, A. A.; Popov, A. A.; Tselikov, G.; Zelepukin, I.; Deyev, S. M.; Kaprin, A. D.; Ivanov, S.; Timoshenko, V. Y.; Prasad, P.N.; Zavestovskaya, I. N.; Kabashin, A.V. Nuclear Nanomedicine Using Si Nanoparticles as Safe and Effective Carriers of 188Re Radionuclide for Cancer Therapy. *Sci. Rep.* **2019**, *9*, 2017.

(50) Qiu, M.; Singh, A.; Wang, D.; Qu, J.; Swihart, M.; Zhang, H.; Prasad, P. N. Biocompatible and Biodegradable Inorganic Nanostructures for Nanomedicine: Silicon and Black Phosphorus. *Nano Today.* **2019**, *25*, 135-155.

(51) Li, K.; Liu, Y.; Pu, K.-Y.; Feng, S.-S.; Zhan, R.; Liu, B. Polyhedral Oligomeric Silsesquioxanes-Containing Conjugated Polymer Loaded PLGA Nanoparticles with Trastuzumab

(Herceptin) Functionalization for HER2-Positive Cancer Cell Detection. *Adv. Funct. Mater.* **2011**, *21*, 287–294.

(52) Lee, Y.-H.; Chang, D.-S. Fabrication, Characterization and Biological Evaluation of Anti-HER2 Indocyanine Green-Doxorubicin-Encapsulated PEG-b-PLGA Copolymeric Nanoparticles for Targeted Photochemotherapy of Breast Cancer Cells. *Sci. Rep.* **2017**, *7*, 453.

(53) Thuy Le, Duong Thi. Anti-Tumor Activity of Docetaxel PLGA-PEG Nanoparticles with a Novel Anti-HER2 scFv. *J. Nanomed. Nanotechnol.* **2015**, *06*.

(54) Shipunova, V. O.; Nikitin, M. P.; Mironova, K. E.; Deyev, S. M.; Nikitin, P. I. Complexes of Magnetic Nanoparticles and scFv Antibodies for Targeting and Visualizing Cancer Cells. In *Proceedings of the 15th IEEE International Conference on Nanotechnology (IEEE-NANO)*; Rome, Italy, 27-30 July; IEEE, 345 E 47TH ST, New York, NY 10017 USA, 2015, 13–16.

(55) Shipunova, V. O.; Zelepukin, I. V.; Stremovskiy, O. A.; Nikitin, M. P.; Care, A.; Sunna, A.; Zvyagin, A. V.; Deyev, S. M. Versatile Platform for Nanoparticle Surface Bioengineering Based on SiO_2-Binding Peptide and Proteinaceous Barnase*Barstar Interface. *ACS Appl. Mater. Interfaces* **2018**, *10*, 17437–17447.

(56) Makita-Chingombe, F.; Kutscher, H. L.; DiTursi, S. L.; Morse, G. D.; Maponga, C. C. Poly(lactic-Co-Glycolic) Acid-Chitosan Dual Loaded Nanoparticles for Antiretroviral Nanoformulations. *J. Drug Delivery* **2016**, *2016*, 1–10.

(57) Studier, F. W. Protein Production by Auto-Induction in High Density Shaking Cultures. *Protein Expression and Purif.* **2005**, *41*, 207–234.

(58) Shipunova, V. O.; Nikitin, M. P.; Nikitin, P. I.; Deyev, S. M. MPQ-Cytometry: A Magnetism-Based Method for Quantification of Nanoparticle–Cell Interactions. *Nanoscale* **2016**, *8*, 12764–12772.

(59) Shramova, E. I.; Proshkina, G. M.; Chumakov, S. P.; Khodarovich, Y. M.; Deyev, S. M. Flavoprotein MiniSOG Cytotoxisity Can Be Induced by Bioluminescence Resonance Energy Transfer. *Acta Naturae* **2016**, *8*, 118–123.

(60) Proshkina, G. M.; Shramova, E. I.; Shilova, O. N.; Ryabova, A. V.; Deyev, S. M. Phototoxicity of Flavoprotein MiniSOG Induced by Bioluminescence Resonance Energy Transfer in Genetically Encoded System NanoLuc-miniSOG Is Comparable with Its LED-Excited Phototoxicity. *J. Photoh. Photobio. B* **2018**, *188*, 107–115.

(61) Richter, M.; Yumul, R.; Wang, H.; Saydaminova, K.; Ho, M.; May, D.; Baldessari, A.; Gough, M.; Drescher, C.; Urban, N.; Roffler, S.; Zubieta, C.; Carter, D.; Fender, P.; Lieber, A. Preclinical Safety and Efficacy Studies with an Affinity-Enhanced Epithelial Junction Opener and PEGylated Liposomal Doxorubicin. *Mol. Ther. Methods Clin. Dev.* **2015**, *2*, 15005.